Contrib Mineral Petrol (2000) 139: 436–457

Maria Teresa Gómez-Pugnaire
Peter Ulmer · Vicente López-Sánchez-Vizcaíno

Petrogenesis of the mafic igneous rocks of the Betic Cordilleras: A field, petrological and geochemical study

Received: 5 July 1999 / Accepted: 28 February 2000

Abstract Mafic igneous rocks are widespread in the Nevado-Filábride Complex, the lowermost metamorphic unit of the internal zones of the Betic Cordilleras. They form intrusive, small, discontinuous bodies, predominantly dikes with subordinate small lava flows. The entire complex underwent alpine compressional metamorphism during the Paleogene continental collision, resulting in eclogites and blueschists in the mafic bodies and high-pressure assemblages in the intruded metasediments. Locally, weakly metamorphosed or completely unmetamorphosed igneous rocks with the same textural features occur as patches surrounded by eclogitized igneous rocks. The bulk rock chemistry of unmetamorphosed and completely metamorphosed mafic igneous rocks is consistent with an alkaline to transitional tholeiitic magmatism with typical within-plate geochemical characteristics. All but a few samples are nepheline normative and display REE and trace element characteristics typical of continental, rift-related magmatism. This conclusion is strongly supported by the mineral chemistry of the major constituents, in particular the calcic Ti-rich character of clinopyroxene, the lack of orthopyroxene, and the occurrence of kaersutitic amphibole. Incompatible trace element abundances and Sr and Nd isotopes support the provenance of these magmas from a variably metasomatized previously depleted sub-continental lithospheric mantle source.

Supplementary material Table 1 Representative olivine analyses, Table 2 Representative clinopyroxene analyses, Table 3 Representative amphibole analyses, Table 4 Major (wt%) and trace element (ppm) contents of Nevado-Filábride mafic rocks, have been deposited in electronic form and can be obtained from http://link.springer.de/link.service/journals/00410

M. T. Gómez-Pugnaire (✉)
Departamento de Mineralogía y Petrología,
Universidad de Granada, Avd. Fuentenueva s/n.,
18002 Granada, Spain
e-mail: teresa@goliat.ugr.es
Tel.: +34-958-243358; Fax: +34-958-243368

P. Ulmer
Department of Earth Sciences, ETH-Zurich,
Sonneggstr. 5, 8092 Zurich, Switzerland

V. López-Sánchez-Vizcaíno
Departamento de Geología, Universidad de Jaén,
Escuela Universitaria Politécnica,
Calle Alfonso X el Sabio 28, 23700 Linares, Spain

Editorial responsibility: V. Trommsdorff

Introduction

The origin and geotectonic significance of the Mesozoic basic igneous rocks that occur in the Nevado-Filábride Complex (NFC hereinafter), the lowermost metamorphic complex of the internal zones of the Betic Cordilleras, are still debated. Previous studies of the mafic igneous rocks of the Betic Cordilleras (e.g. Bodinier et al. 1987; Puga et al. 1989, 1995) have favored an interpretation of these mafic rocks as part of an ophiolitic rock association (''Betic Ophiolitic Association''). The results of the present study are not compatible with such an interpretation and the present petrographic and geochemical constraints indicate a continental within-plate type magmatism associated with crustal-thinning.

The NFC (Fig. 1) consists of two main units: (1) the lower Veleta nappe (Puga et al. 1974), composed exclusively of graphite-bearing metasediments, presumably of Paleozoic (Lafuste and Pavillon 1976) and Precambrian age (Gómez-Pugnaire et al. 1982); and (2) the upper Mulhacén nappe (Puga et al. 1974), comprising of Paleozoic and older basement rocks overlain by a shallow marine metasedimentary cover. The basic igneous rocks occur exclusively in the cover of the upper Mulhacén unit, where they form small, discontinuous, intrusive bodies, predominantly dikes, with subordinate small lava flows.

Both the igneous and sedimentary rocks from the Mulhacén nappe underwent alpine compressional metamorphism during the Paleogene continental collision, resulting in eclogites and blueschists in the mafic bodies and high-pressure assemblages in the metasediments. The decompressional metamorphic path evolved

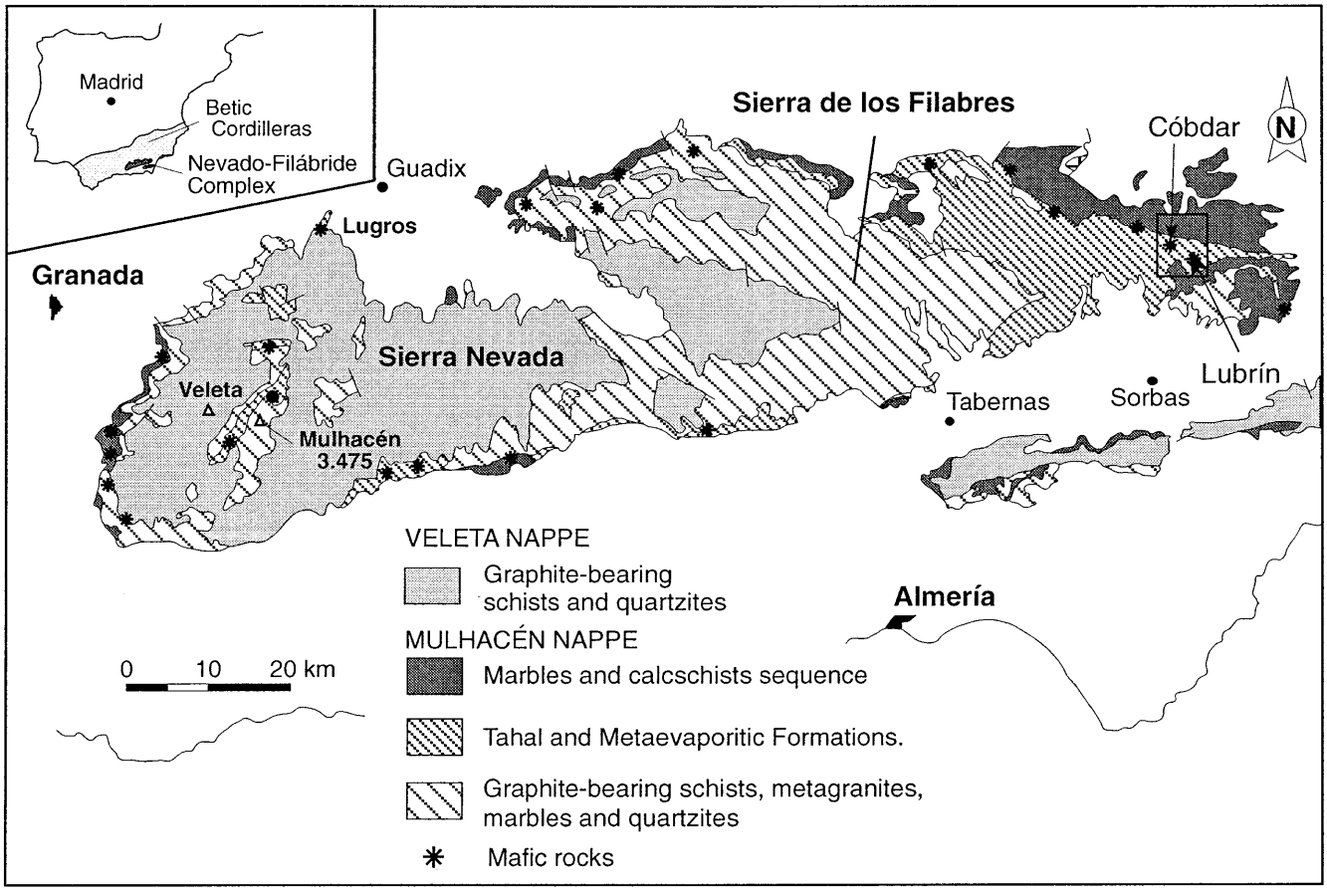

Fig. 1 Geologic map of the Nevado-Filábride Complex forming part of the Sierra Nevada and Sierra de los Filabres in SE Spain (modified from López-Sánchez-Vizcaíno, 1994). The localities mentioned in the text are given for reference. The studied area is outlined with a *box*; the *asterisks* show the main Nevado-Filábride metabasites outcrops

at almost isothermal conditions towards amphibolite facies and greenschist facies conditions (Platt and Behrmann 1986; Gómez-Pugnaire and Fernández-Soler 1987) although a late thermal overprinting has also been proposed (Vissers 1981; Bakker et al. 1989).

Ductile deformation related to the uplift affected the eclogites in local shear zones and produced foliated mafic schists. In contrast, most of the eclogites in the low-strain zones preserve their igneous textures and original intrusive contacts with the metasediments. Moreover, some igneous protoliths of the eclogites locally escaped the high-pressure metamorphism, displaying the unmodified igneous fabrics and mineralogy. Both the igneous protoliths and the surrounding eclogites contain continental crustal xenoliths. The latter consist of large andalusite crystals, fragments of metacarbonates and microfolded metapelites, which have been partially assimilated by the host magma (Gómez-Pugnaire and Muñoz 1991). Utilizing geological and geochemical data, we will argue that the basic rocks of the NFC represent the products of alkaline to transitional magmatism in an extensional environment possibly related to a Jurassic rifting event, as suggested by radiometric data (Hebeda et al. 1980; Puga et al. 1995).

Former interpretation

Bodinier et al. (1987) and Puga et al. (1989, 1995) consider the Nevado-Filábride basic rocks, and particularly those of the Cóbdar area, as part of a tectonic unit which would represent a dismembered oceanic crust, the so-called "Betic Ophiolitic Association" (Puga et al. 1989). In its original definition this ophiolitic nappe consisted of ultramafic rocks ("the ophiolitic harzburgites", Morten and Puga 1984) crosscut by small bodies of cumulate gabbro and basic dikes, rodingitized in many cases, covered by volcanic rocks with pillow structures (Puga et al. 1995). The top of the sequence in the Cóbdar area consists, according to these latter authors, of thin calcareous layers of the Marble and Calcschists formation (Tendero et al. 1993). They base their interpretation on the occurrence of some "ankeritic objects" that they interpret as Cretaceous planktonic foraminifers. However, as pointed out by Gómez-Pugnaire et al. (2000), most of these "objects" do not have a morphology attributable to any type of fossils. In addition, even if trochospiral coiling were responsible for these "planktonic-foraminifer profiles," such coiling is also common in benthic foraminifers from a wide geological time span.

The composition of basic igneous rocks reported by Puga et al. (1989) for the Cóbdar area is very similar to those presented here: two sequences of rocks, exhibiting alkaline to transitional geochemical characteristics. For these rocks, Bodinier et al. (1987) and Puga et al. (1989, 1995) propose several possible origins: (1) under *P*-type-ridge geodynamic conditions, (2) at a spreading center in a back-arc marginal basin, or (3) at a small Red Sea-type basin. Puga et al. (1989) even suggest that local continental contamination occurred "during the early stages of the oceanic basin opening or else by their intrusion along the continental margin of this basin".

Finally, the significance of the ultramafic bodies is of great importance for resolving the origin of the magmatism and the tectonic evolution of the NFC. In the Cóbdar area, there are no ultramafic rocks associated with the studied basic rocks. The closest ultramafic bodies occur some kilometers to the north as serpentinite lenses with very variable size and in the same stratigraphic position in the upper part of the sequence. This is also the case for the large ultramafic bodies of the NFC, that appear in Sierra Nevada and Sierra de Baza (about 100 km to the west) associated with rodingitized basic rocks.

Puga et al. (1989) interpreted the serpentinized ultramafic rocks as sub-oceanic harzburgites. However, such an interpretation is inconsistent with a recent study by Trommsdorff et al. (1998) and Puga et al. (1999). The former authors showed that the serpentinites derive from lherzolitic compositions, which locally were transformed to Al-rich harzburgites by extensive serpentinization (loss of Ca, as evidenced by the formation of rodingites). Based on their study, Trommsdorff et al. (1998) prefer a sub-continental lithospheric origin of these hydrated ultramafic rocks. The geochemical character and the tectonic position of these ultramafic rocks render it very unlikely that they could represent the partial melting residua of the basic igneous rocks observed in the NFC. Most likely, the ultramafic lenses were tectonically incorporated into the NFC well before the onset of the basic magmatism.

In the following chapters we present evidence that the occurrence of spatially separated serpentinized ultramafic rocks and basic igneous hypabyssal-to-subvolcanic rocks that form gabbroic bodies and dikes do not constrain an oceanic ophiolite type rock association, but represent two independent events: tectonic incorporation of sub-continental lithospheric mantle followed by a crustal-extension related, basic transition to tholeiitic magmatism.

Geological setting and field relationships

The majority of the investigated samples belong to the Sierra de los Filabres and outcrop near Cóbdar (Fig. 1). In this area, eclogites and remnants of the unmetamorphosed igneous protoliths occur side by side. The almost complete lack of deformation permits the observation of relationships among the different magmatic injections and the relations to the surrounding metasediments (Muñoz 1986; Franz et al. 1988). In the nearby village of Lubrín, the metabasite occurrence is very similar to that of Cóbdar, although less well exposed (Morten et al. 1987).

The age of the intrusion has been dated with a Rb-Sr mineral isochrone for an unmetamorphosed gabbro from the Cóbdar area yielding 146 ± 4 Ma (Hebeda et al. 1980). K-Ar determinations on a similar sample from the same area resulted 174 – 164 ± 4 Ma (Portugal-Ferreira et al. 1988). A middle- to late-Jurassic age of the basic intrusions in the Mulhacén unit is consistent with the general tectonic framework of a continental rifting proposed for the Betic Cordilleras (see De Jong 1991). However, there is still considerable debate on the subject of how this extensional stage evolved: (1) toward an open ocean basin (Puga et al. 1989), (2) local oceanic pull-apart basins (De Jong 1991), or (3) as an aborted continental rift (Muñoz 1986; Franz et al. 1988; Gómez-Pugnaire 1981).

Lithostratigraphic features of the intruded metasediments

Basic rocks intrude a (< 1000 m thick) metasedimentary sequence belonging to the so-called Nevado-Lubrín Unit (Nijhuis 1964). This sequence is constituted (Fig. 2) by:

1. The *Tahal schist formation* (Nijhuis 1964). It consists of a thick (ca. 1000 m) sequence of quartzite layers (up to 1–3 m thick) alternating with relatively low proportions of light-colored quartz-feldspar micaschists, locally garnet-, chloritoid- and/or amphibole-bearing. At the base, overlying the graphite-rich quartzite and micaschist sequence of the basement, discontinuous, scarce outcrops of metaconglomerates appear (Egeler 1963; Gómez-Pugnaire et al. 1982; De Jong and Bakker 1991).
2. The *Metaevaporite (MEV) formation* (Gómez-Pugnaire et al. 1994). This is a thin (up to 80 m, usually less than 20 m) discontinuous formation that overlies the Tahal schists. It consists of scapolite-gypsum-bearing marbles (Nijhuis 1964; Voet 1967; Gómez-Pugnaire 1981; Soto 1993), calcschists, quartzites, and fine-grained scapolite-gypsum-anhydrite-barite-bearing metapelites (Gómez-Pugnaire et al. 1994) that also display the high-pressure assemblage kyanite-talc-phengite.
3. The *Marble and Calcschist formation* (Voet 1967). It consists predominantly of laminated and massive calcitic and dolomitic marbles (up to 300 m), with some intercalations of calcschists, quartzites, and basic and ultrabasic rocks (López-Sánchez-Vizcaíno 1994). The modal abundance of carbonate increases progressively upwards, with a thick (75–100 m) sequence of almost massive calcitic and dolomitic marbles at the top. Some layers of carbonate-free, kyanite-, chloritoid- and staurolite-bearing micaschists appear at the base of the formation.

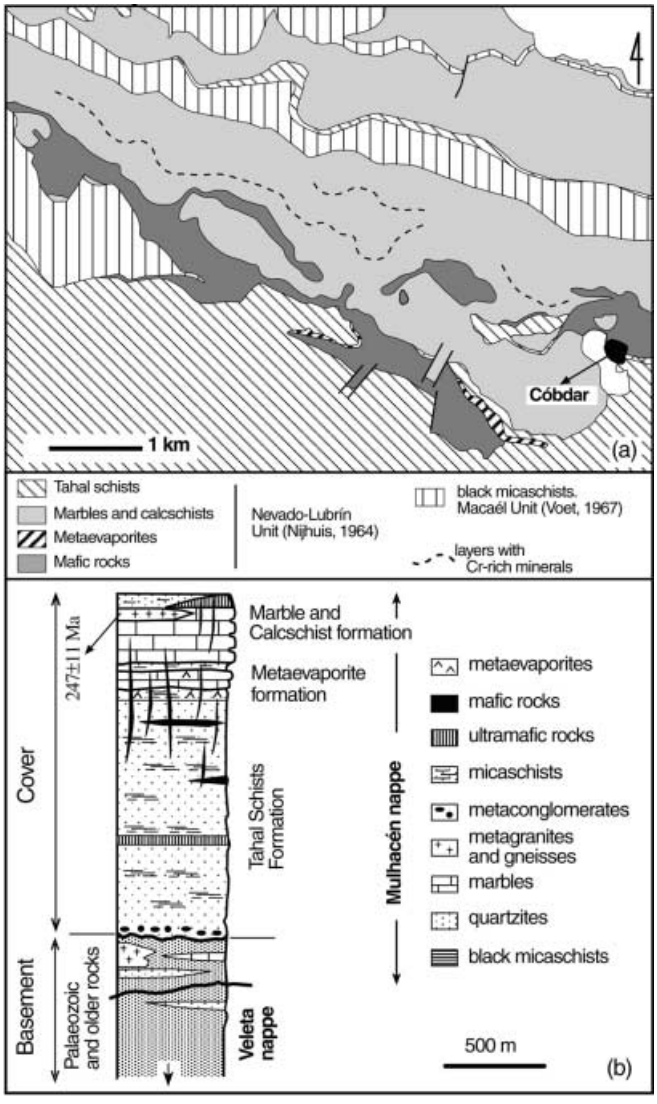

Fig. 2 **a** Tectonic map of the Cóbdar area showing the tectonic subdivision of the Nevado-Filábride Complex after Voet (1967) and modified by Gómez-Pugnaire et al. (1994) (addition of the metaevaporitic formation). The location of the Cr-rich layers are taken from López-Sánchez-Vizcaíno (1994); **b** Litho-stratigraphic column of the Nevado-Filábride Complex

The marbles and calcschists may show recurrent intercalations of very thin layers of calcschists consisting of more than 70 vol% of some unusually Cr-rich minerals (epidote, phengite, chlorite, Fig. 2a). The origin of the high Cr content is related to the occurrence of detritic grains of chromite (López-Sánchez-Vizcaíno et al. 1995).

Structural relationships

Numerous studies have dealt with the structure, the number of tectonic units, and the nature of the internal contacts of the NFC, as well as the relationships with the other units of the Betic complexes (Vissers 1981; Martínez-Martínez 1986; Bakker et al. 1989; Vissers et al. 1995; De Jong 1991; Galindo-Zaldívar 1993; Jabaloy 1993; Soto 1993 among others). The following paragraphs concentrate on the cover formations where the studied basic rocks intruded.

From a structural point of view, the graphite-bearing metasediments attributed to the Paleozoic and the three formations described above constitute a single tectonic unit representing the original stratigraphic sequence of the NFC (Nijhuis 1964; Voet 1967; Gómez-Pugnaire 1981; De Jong and Bakker 1991; Jabaloy 1993).

There is no proof that the contact between Tahal schists and MEV formations corresponds to a detachment zone during the main syn-metamorphic deformational stages or during the post-metamorphic Miocene extensional faults (Platt 1986; Platt and Behrmann 1986; García-Dueñas et al. 1988; Galindo-Zaldívar et al. 1989; Platt and Vissers 1989; Aldaya et al. 1991; Comas et al. 1992; Watts et al. 1993). Furthermore, the original stratigraphic relationships have remained essentially undisturbed (Gómez-Pugnaire 1981; De Jong and Bakker 1991; Jabaloy 1993; López-Sánchez-Vizcaíno 1994). We favor the interpretation that the penetrative brecciation resulting in gypsum being squeezed out during and after deformation (Leine 1966) was driven by the contrasting rheology of the lithologies involved. Most probably, this mechanism started immediately after deposition of the sediments during compaction and diagenesis.

Igneous rocks

The basic igneous rocks mainly occur in the transition zone between the Tahal schists and the Marbles and Calcschist formation (Fig. 2), and less commonly within the Tahal schists. Most basic rocks consist of undeformed, blastoporphyritic, amphibolitized eclogites with well preserved gabloroidic or doleritic igneous textures. More rarely, less preserved eclogites occur where augite relics represent the only remnants of the original igneous mineralogy.

Locally, weakly metamorphosed or unmetamorphosed igneous rocks with the same textural features occur as patches surrounded by the blastoporphyritic eclogites. The contact between both lithologies is usually sharp and easily recognizable in the field by their different colors: green for the amphibolitized eclogites and dark-brown for the igneous relics. Where unaltered igneous rocks occur, field relationships unambiguously indicate that they were the protoliths of the amphibolitized eclogites. These unmetamorphosed igneous rocks are rare in the NFC: All the known localities are restricted to the Sierra de los Filabres (Fig. 1), and especially to the Cóbdar area, where the largest and most representative outcrops are found.

The intrusive features, still recognizable in the igneous rocks and their metamorphic analogues, such as chilled margins, flow alignment of phenocrysts and cooling joint structures, are typical of subparallel mul-

tiple-injection dikes, crosscutting the Tahal coastal clastic metasediments, the metaevaporites (Fig. 3a) and the marbles (Gómez-Pugnaire 1981; Muñoz et al. 1988; Franz et al. 1988; De Jong and Bakker 1991). Dike textures range from gabbroic to doleritic with variable grain-size, to porphyritic, to aphanitic-vesicular with a very-fine matrix (Fig. 3a–c). The gabbroic rocks constitute the core of the largest dikes (1–20 m thick), whereas the doleritic rocks are typical of the chilled margins or of small dikes (up to 1 m thick). The porphyritic and aphanitic-vesicular facies occur in the thinner dikes (from 2 to 50 cm; Fig. 3b–d). In the largest dikes (up to 20 m) an increase in grain size is commonly observed toward the inner parts. Fine- to very fine-grained dolerite form the dike margins, and medium- to coarse-grained gabbroic rocks appear in the internal portions. The latter have been produced by the differential accumulation of predominantly large olivine and subordinate plagioclase crystals. The occurrence of differential accumulation of minerals in the central part of the bodies, and their parallelism to the margins, point towards an origin controlled by flow differentiation. Brittle deformation, linked to post-metamorphic joints, induced the brecciation of some relatively large dikes (2–3 m thick) and occasionally the formation of rounded blocks described as pillow-lavas by Puga et al. (1989). The outcrop features, however, clearly indicate that the supposed pillow-lavas are merely fragments of porphyritic dikes bounded by joints or even onionskin weathered blocks. The massive vesicular basalts enclosing the pillow-lavas described by Puga et al. (1989) correspond to the unbrecciated portion of the same fine-grained dikes (Gómez-Pugnaire and Muñoz, 1991).

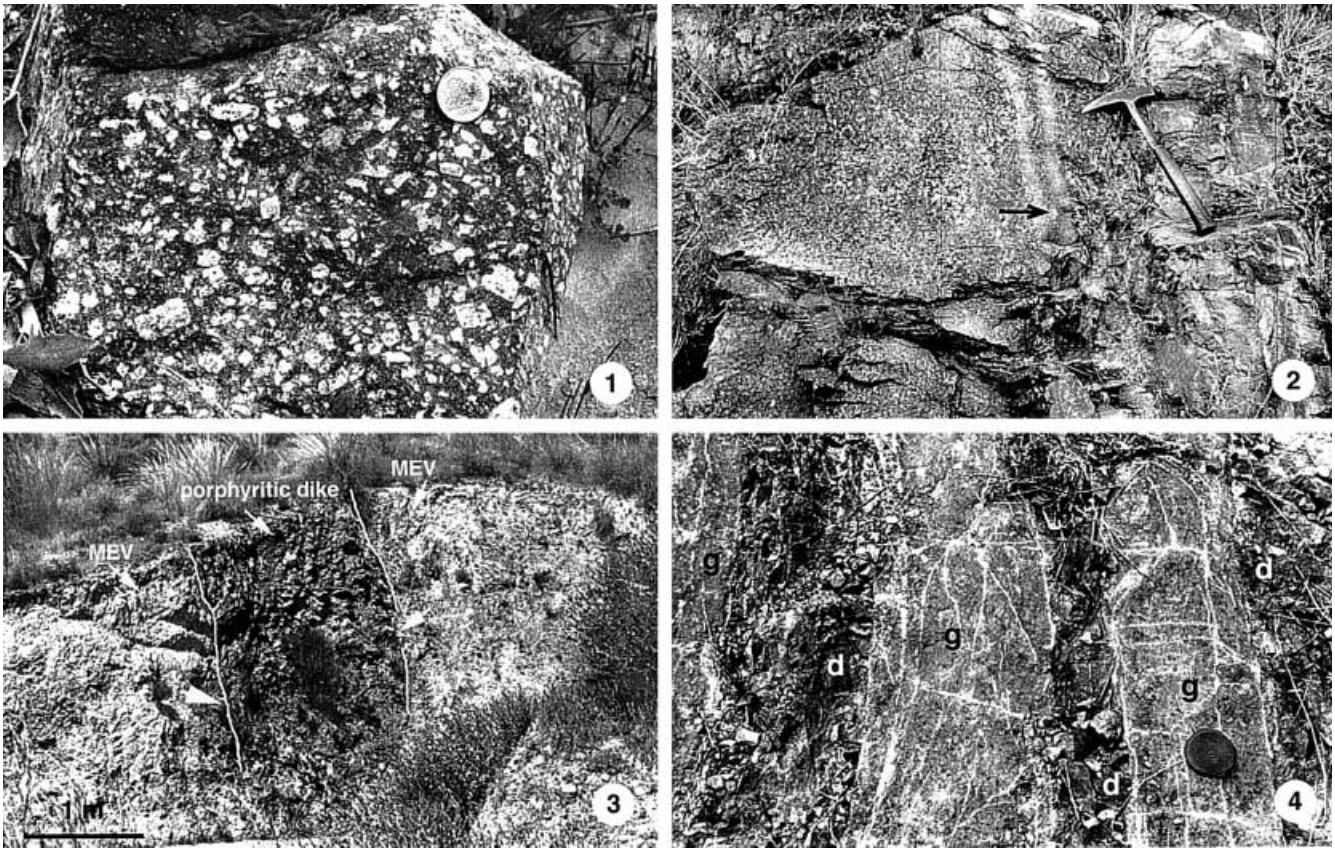

Fig. 3 **1** Porphyritic dike rock sample that contains abundant large phenocrysts of plagioclase in a nearly aphyric matrix; **2** Two generations of dike rocks: The large porphyritic dike is crosscut by two very fine-grained (nearly aphyric) dikes, one of them displays phenocrysts (plagioclase) accumulation in the central part (see *arrow*); **3** Porphyritic dike with rare, small plagioclase phenocrysts crosscutting the metapelites of the Metaevaporite formation (MEV) that contains (not visible in the picture) abundant scapolite porphyroblasts and gypsum pseudomorphs; **4** Olivine-rich gabbro (*light gray*, *g*) intruded by several very-fine grained dikes (*dark gray*, *d*) that contain rare plagioclase phenocryst. The white veins are replenished by late scapolite

Petrography

Unmetamorphosed basic igneous rocks

Gabbroic and doleritic dikes are massive rocks, with variable grain size and textures depending on the dike thickness, the existence of cumulate structures, and the presence of chilled margins.

1. *Coarse-grained gabbroic rocks (average grain size = 2–3 mm)* are cumulate rocks that occur in the central parts of the largest dikes. Most of these rocks contain large crystals of cumulus olivine (30–35%),

and/or plagioclase (30–35%) and sparse ilmenite and Ti-magnetite in a medium-grained ophitic to subophitic matrix consisting of clinopyroxene (15–20%), tabular plagioclase (10–15%), Ti-rich amphibole (5–10%), and occasionally Ti-rich biotite (0.5–2%). Olivines appear as dark brown euhedral to rounded, and rarely skeletal, crystals. Occasionally, olivines are concentrated in layers alternating with layers formed predominantly by weakly zoned plagioclase phenocrysts. Clinopyroxene has not been observed as a phenocryst phase. Most frequently, clinopyroxene forms large poikilitic grains, with colorless or greenish cores, reddish rims, and rare sector zoning. Accessory minerals are chromite and pyrite, mostly as inclusions in the olivine phenocrysts, and rarely apatite, zircon and zirconolite.

2. *Fine- to very fine-grained doleritic rocks* are similar to the coarse-grained rocks in that they consist mainly of olivine, and rarely plagioclase microphenocrysts, set in an ophitic to subophitic matrix of reddish-brown clinopyroxene, plagioclase, Ti-amphibole and occasionally olivine and biotite. These rocks include samples from the chilled margins of the largest dikes and from the smaller distinct dikes, which do not generally contain microphenocrysts.
3. *Very fine-grained porphyritic rocks (with partially aphyric mesostasis)* occur as dikes crosscutting the gabbro-dolerite suite (Fig. 3d). They display different textures depending on the thickness and the exact localization of the sample within the dike. Flow differentiates are common in the central part of the dikes (Fig. 3b). Large subhedral or even skeletal crystals of olivine, spinel and, in some cases, plagioclase are surrounded by a fine-grained microcrystalline- (Fig. 3a), intergranular-, intersertal-, and/or subophitic-textured groundmass consisting of plagioclase, clinopyroxene, Ti-rich amphibole, ilmenite and glass. Glomeroporphyritic aggregates of plagioclase and less frequently of olivine are common.

Several generations of dike intrusion can be distinguished in the outcrops; the aphyric dikes form the younger dikes. Angular fragments of very fine-grained/glassy rocks with rare crystal clots of small plagioclase, and medium-grained doleritic fragments, are sometimes enclosed in the porphyritic rock types. In some places, multiply injected porphyritic dikes are separated from each other by lobate surfaces, suggesting that the injection of some of the dikes took place before complete solidification of the previous injection.

Metamorphosed basic igneous rocks

Textural and outcrop features of the blastophyric metabasites are similar to those of the unmetamorphosed counterparts, but the igneous mineralogy has been almost completely obliterated during several metamorphic events (Gómez-Pugnaire and Fernández-Soler 1987; Morten et al. 1987; Franz et al. 1988). The earlier stages of the Alpine metamorphism produced eclogites that transformed progressively into blueschist, amphibolite, and greenschist mineral assemblages during the near isothermal decompression concomitant with the uplift. The contact between metamorphosed and unmetamorphosed basic rocks is generally sharp and steep. From field evidence alone, no explanation can be offered as to why some of these rocks have completely escaped from metamorphism.

Igneous mineral composition (mineral chemistry)

Analytical methods

Major-element analyses of minerals were obtained by wavelength dispersive analyses with a CAMECA electron microprobe at the University of Granada using synthetic standards. Accelerating voltage was 15 keV and sample current was 15 nA. Precision was about $\pm 1.5\%$ relative for a concentration of 1 wt%. Mineral compositions reported in Table 1 are only a representative selection. The complete data set of mineral analyses is presented as Tables 1–3 in the Springer electronic supplementary material accompanying this manuscript.

Olivine

Olivine is the ubiquitous phenocryst phase in all the lithologies and, more rarely, it occurs in the groundmass. All olivine crystals display a peculiar reddish-brown pleochroism; the colored olivines either occur as rims around colorless cores or form entire crystals. Olivine in the matrix is always brown. This unusual color is most probably caused by a large quantity of minute inclusions of chromian magnetite poor in Ti, similar to that described by Trommsdorff et al. (1998). However, to date an unequivocal identification of such inclusions by TEM has not been successful.

Olivine is the liquidus phase in most dikes, as indicated by its euhedral habit and its occurrence as an inclusion in plagioclase and clinopyroxene. Fig. 4 shows the variation of X_{Mg} [$Mg/(Mg + Fe^{2+})$] of "coexisting" olivine and clinopyroxene. According to experimental determinations (e.g. Kawasaki and Ito 1994) the X_{Mg} of clinopyroxene is higher than that of coexisting olivine at igneous temperatures. This is true for all the phenocryst-free doleritic samples and some gabbros, but is strongly violated by the porphyritic rocks and some doleritic samples. The olivines of these latter samples exhibit considerably higher X_{Mg} than clinopyroxene (Table 1) indicating that such olivines are out of equilibrium with the clinopyroxenes that are found exclusively in the matrix. The highest X_{Mg} values (0.83–0.88) correspond to olivine phenocrysts from olivine-bearing porphyritic dikes and from the olivine + plagioclase + clinopyroxene cumulates. The same range of X_{Mg} variation can also be

Table 1 Representative olivine and clinopyroxene analyses

Sample rock	CC-12 dolerite matrix	CB-6/3 dolerite rim	CH-57 gabbro core[a]	CH-49 gabbro rim	CH-49 gabbro core	CB-388 PH[b] rim	CC-12 dolerite	CB-6/3 dolerite rim	CH-49 gabbro core	CH-49 gabbro rim	CB-388 PH[b] rim
SiO_2	38.82	38.06	40.41	37.76	40.36	40.58	47.61	48.15	49.75	51.26	45.43
TiO_2	0.03	0.03	0.00	0.03	0.01	0.01	3.13	2.68	1.43	1.48	3.42
Al_2O_3	0.02	0.00	0.04	0.00	0.07	0.08	5.84	5.08	4.34	2.58	7.00
Cr_2O_3	0.01	0.00	0.03	0.00	0.03	0.05	0.31	0.03	0.75	0.04	0.09
Fe_2O_3[c]	0.00	0.00	0.00	0.00	0.00	0.00	2.26	2.50	1.62	0.99	3.65
FeO	21.86	25.28	12.23	26.05	13.02	11.99	5.12	6.44	5.39	6.38	7.25
MnO	0.31	0.34	0.23	0.42	0.19	0.19	0.14	0.16	0.16	0.22	0.17
MgO	39.25	36.91	46.87	35.47	46.19	47.40	13.52	12.96	14.82	15.05	10.72
NiO	0.10	0.10	0.20	0.09	0.23	0.25	0.00	0.02	0.03	0.03	0.00
CaO	0.26	0.20	0.32	0.12	0.31	0.28	21.28	21.16	20.36	20.70	21.28
Na_2O	0.00	0.01	0.02	0.04	0.01	0.01	0.67	0.67	0.58	0.56	0.77
K_2O	0.01	0.01	0.01	0.00	0.01	0.01	0.01	0.01	0.01	0.02	0.02
Total	100.66	100.95	100.34	99.96	100.41	100.85	99.68	99.85	99.07	99.19	99.4
Cations normalized on 4 oxygens (olivine) and 4 cations and 6 oxygens (clinopyroxene)											
Si	1.001	0.996	1.000	1.002	1.001	0.998	1.772	1.802	1.852	1.908	1.722
Al^{IV}	–	–	–	–	–	–	0.228	0.198	0.148	0.092	0.278
Al	0.001	0.000	0.001	0.000	0.002	0.002	0.029	0.026	0.043	0.022	0.034
Cr	0.000	0.000	0.001	0.000	0.001	0.001	0.009	0.001	0.022	0.001	0.003
Ti	0.001	0.001	0.000	0.000	0.000	0.000	0.088	0.075	0.040	0.041	0.097
Fe^{3+}	–	–	–	–	–	–	0.063	0.071	0.045	0.028	0.104
Fe^{2+}	0.471	0.553	0.253	0.578	0.270	0.247	0.159	0.202	0.168	0.199	0.230
Mn	0.007	0.007	0.005	0.009	0.004	0.004	0.005	0.005	0.005	0.007	0.005
Mg	1.508	1.439	1.728	1.402	1.707	1.737	0.750	0.723	0.822	0.835	0.605
Ni	0.002	0.002	0.004	0.002	0.004	0.005	0.000	0.000	0.001	0.001	0.000
Ca	0.007	0.006	0.008	0.003	0.008	0.007	0.849	0.848	0.812	0.826	0.864
Na	0.000	0.000	0.001	0.002	0.000	0.000	0.048	0.049	0.042	0.040	0.056
K	0.000	0.000	0.000	0.000	0.000	0.000	0.001	0.000	0.000	0.001	0.001
X_{Mg}[d]	0.76	0.72	0.87	0.71	0.86	0.88	0.82	0.78	0.83	0.81	0.72

[a] Partially metamorphosed sample
[b] *PH* porphyritic sample
[c] Fe_2O_3 of clinopyroxene recalculated on the basis of stoichiometry and charge balance
[d] $X_{Mg} = [Mg/(Mg + Fe^{2+})]$

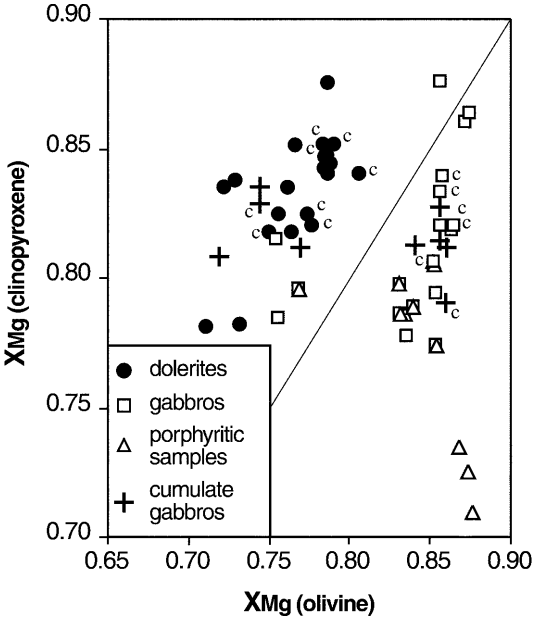

Fig. 4 Partitioning of X_{Mg} [$=Mg/(Mg + Fe^{2+})$] between olivine and clinopyroxene. The *line* indicates equal X_{Mg} of olivine and clinopyroxene. Samples plotting below the line (low X_{Mg} of the clinopyroxene relative to that of olivine) indicate disequilibrium (c = core of the olivine crystals)

found in single-zoned olivine phenocrysts. These olivines are primocrysts, originating from earlier differentiation stages and have accumulated during subsequent differentiation. Crystal retention ultimately led to the extremely Mg-enriched character of some bulk rock samples. The plot of forsterite content versus X_{Mg} of bulk-rock (Fig. 5) shows that the compositions of olivine usually plot below the experimentally derived partitioning relationship between olivine and basaltic liquid (Roeder and Emslie 1970; Ulmer 1989). Such relationships indicate an accumulation of early-crystallized olivines. In rocks with seriate porphyritic textures, a continuous decrease in X_{Mg} of olivine from the large phenocrysts to the matrix-grains is observed, indicating a partial equilibration of the primocrysts with the matrix compositions. NiO content in olivine decreases with differentiation from 0.26 wt% NiO ($X_{Fo} = 0.86$) in the most Mg-rich rocks (olivine-bearing porphyritic dikes and cumulates) to less than 0.1 wt% NiO in the more evolved dolerites and plagioclase-bearing porphyritic rocks ($X_{Fo} = 0.68$–0.75). The compositional variations of olivine are consistent with crystallization from near primary mantle-derived basalt magmas and subsequent low-pressure differentiation (e.g. Simkin and Smith 1970).

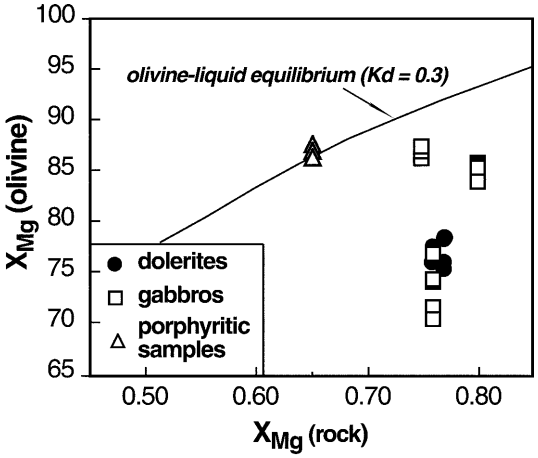

Fig. 5 Partitioning of X_{Mg} between olivine and the bulk. The *line* corresponds to the equilibrium partitioning between olivine and liquid at 1 bar (Roeder and Emslie 1970; Ulmer 1989). Samples plotting below the equilibrium line indicate olivine accumulation

Clinopyroxene

Clinopyroxene (cpx) composition ranges between $Wo_{41–44}$, $En_{35–47}$, and $Fs_{7–18}$ (Table 1). Clinopyroxenes show strongly variable Al_2O_3 (2.58–7.00 wt%) and TiO_2 contents (0.95–4.00 wt%) and high CaO (19.66–21.84 wt%). The compositional range of Ti covers – almost completely – the field of within-plate alkaline rocks (e.g. Nisbet and Pearce 1977; Leterrier et al. 1982; Azambre et al. 1992) (Fig. 6a, b). The excellent positive correlation between $Al^{IV}$and Ti (Fig. 6c) with $Al^{IV}/Ti \approx 3$ indicates that the incorporation of Ti in clinopyroxene can exclusively be attributed to a Ti-Tschermak's substitution plus an additional Ca-Tschermak's subtraction. X_{Mg} of cpx correlates negatively with Al^{IV} and Ti (Fig. 6b, d). Such correlations are common in basaltic clinopyroxenes reflecting the preference of Mg^{2+}over Fe^{2+} in the M_1 site and hence the preferred exchange of Mg during Tschermak's substitution.

The Ca-rich composition of the clinopyroxene, as well as the lack of orthopyroxene or pigeonite exolution lamellae, indicates low SiO_2 activity in the melt during crystallization of the Ti-Al^{IV}-rich cpx. Such compositional relationships are typical of low-pressure cpx crystallized from transitional to alkaline basalts (e.g. Gupta et al. 1973). High Al- and Ti-clinopyroxene have also been interpreted as the products of quench crystallization during rapid cooling (Schiffman and Lofgren 1982). However, experimentally produced quench clinopyroxenes display not only high Al and Ti contents,

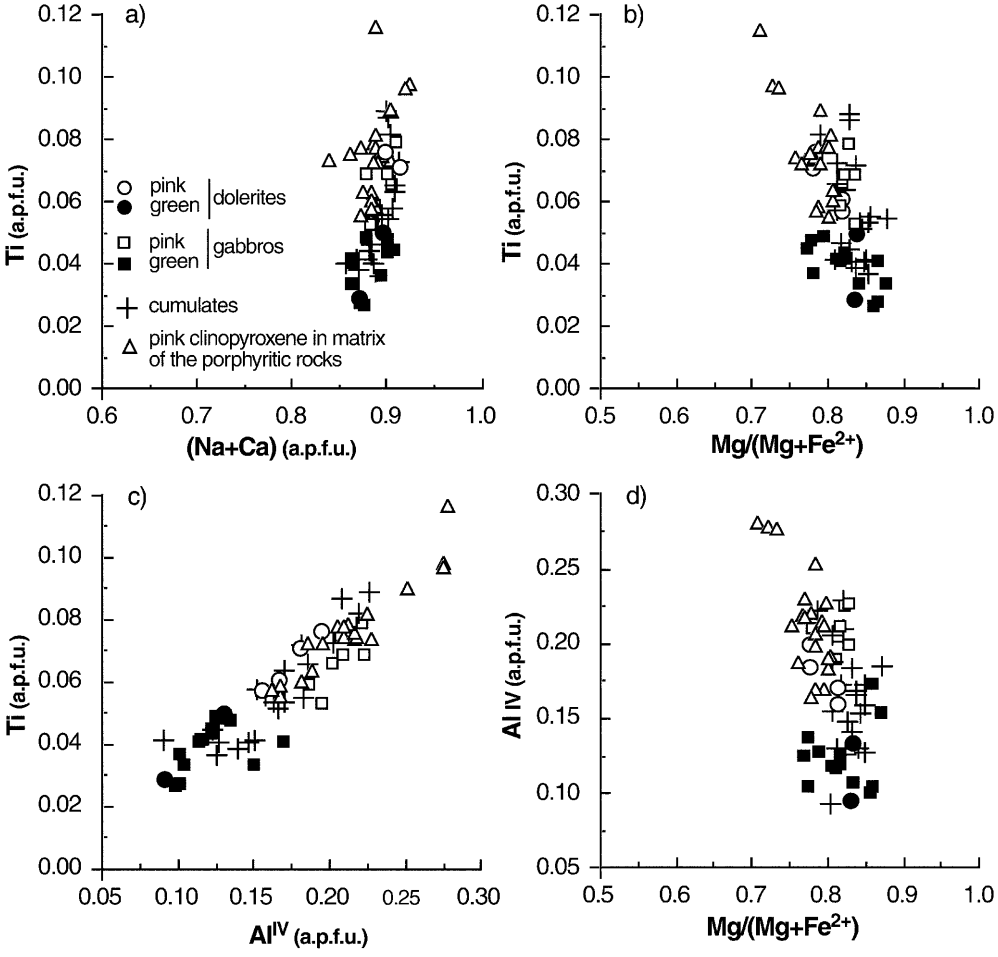

Fig. 6 Variations of clinopyroxene compositions in terms of Ti, Al^{IV} (=2-Si), and Mg/(Mg + Fe^{2+}) (=X_{Mg}). Note that the green clinopyroxene-cores have lower Ti and Al^{IV} contents and higher X_{Mg} than the late-crystallized pink clinopyroxene

but low Ca-contents, not observed in the samples investigated (e.g. Sisson and Grove 1993).

The most primitive clinopyroxene compositions refer to the core of large poikilitic crystals from gabbros and dolerites. These crystals display pale green color and Si-, Mg- and Cr- (up to 1 wt%) rich cores rimmed by pink Al-, Ti-, Na-rich mantles (Fig. 6b, d). Matrix clinopyroxenes in the porphyritic dike rocks are always Al-Ti-rich (see Table 1). Similarly, zoned clinopyroxenes are relatively common in alkaline basalts; they are interpreted as early liquidus phases in equilibrium with the host liquid at high pressures or alternatively as xenocrysts of mantle origin (e.g. Duda and Schmincke 1985; Dobosi 1989). The lack of xenoliths other than those of crustal origin in the studied rocks and the often euhedral shape of the low-Al^{IV} cores argue for a low-pressure origin. Cr-clinopyroxene systematically forms the core of large crystals and exhibits high Mg ($X_{Mg} = 0.75$–0.88) and Cr contents (0.019–0.021 p.f.u.). This suggests that such cpx cores are early precipitates (probably formed at higher pressure than the rims) from near primary liquids.

Plagioclase

Plagioclase compositions in the dolerites ranges from An_{77} to An_{30}, comparable to the range (An_{80}–An_{30}) found in the phenocrysts from the olivine- and plagioclase-bearing porphyritic rocks, and from the gabbros. The large range of plagioclase compositions observed in these samples suggests that the matrix and intercumulus plagioclase crystallized under near equilibrium conditions from their respective liquids. Usually plagioclase microlites show normal zoning with cores up to 15 mol% An richer than the rims. The largest plagioclase crystals from gabbros occasionally exhibit oscillatory or reverse zoning patterns. Rare albitized rims ($An_{5–9}$) are observed. Plagioclase phenocrysts in most of the porphyritic rocks, however, display penetrative albitization that renders impossible the microprobe analyses of these samples.

Amphibole

Amphiboles systematically overgrow and mantle pre-existing clinopyroxene. They are kaersutites ($X_{Mg} = 0.60$–0.80, $Ti = 0.50$–0.70 a.p.f.u.) and brown Ti-rich hastingsites ($X_{Mg} = 0.62$–0.58, $Ti = 0.15$–0.48 a.p.f.u.). They occasionally display a rim of green amphibole of variable composition, which may have formed during metamorphism ($X_{Mg} = 38$–96, $Ti = 0.02$–0.11). Igneous amphiboles do not show continuous trends but exhibit a limited variability in X_{Mg} that is very restricted compared with the compositional variation observed in olivine and clinopyroxene. The lack of sympathetic trends with olivine or clinopyroxene might reflect formation of the amphiboles near the solidus or in the subsolidus by solid state reactions driven by increasing water pressure at the final stage of crystallization.

Biotite

This is a rare mineral which appears as thin and discontinuous rims on amphibole and lacks any distinct zoning pattern, but varies in composition from grain to grain. The compositions range from Ti-bearing phlogopite to Fe-poor biotite ($X_{Mg} = 0.58$–0.84, $Ti = 0.13$–0.53 a.p.f.u.).

Oxide minerals

Chromiferous spinels

Chromium-rich spinels occur as euhedral inclusions in olivine primocrysts and more rarely as matrix constituents. The spinel compositions vary from picotite [$y_{Cr} = Cr/(Cr + Al) = 0.18$; $X_{Mg} = 0.70$] to ferro-chromites ($y_{Cr} = 0.55$; $X_{Mg} = 0.16$). Coexisting olivine-spinel pairs show systematic variations: A negative correlation of the forsterite content with y_{Cr} (spinel) is consistent with continuous equilibration of olivine and spinel during differentiation (Fig. 7). Highly evolved liquids crystallizing olivine Fo_{76} contain ferro-chromites, whereas near primary liquids (Fo_{88}) contain picotitic spinels that suggest temperatures of ca. 1200 °C for the olivine-spinel Fe-Mg exchange geothermometer (Fujii 1977; Engi 1983; Li et al. 1995).

Fe-Ti oxides

Ilmenite and subordinate ulvöspinel form the oxide paragenesis in the matrix of the primitive to evolved basic dikes. Coexisting ilmenite and ulvöspinel pairs from a primitive porphyritic dike rock (CH-32, Fo_{88}) have been used to calculate temperatures and f_{O2}

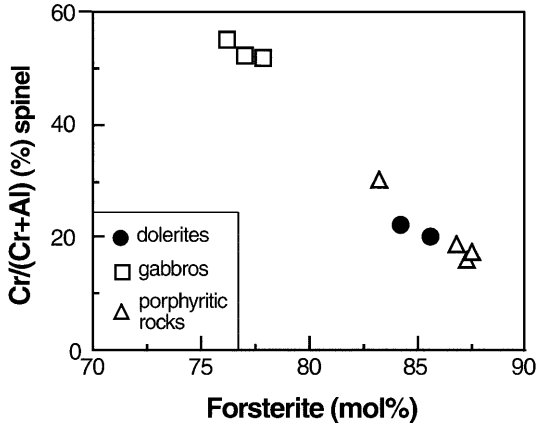

Fig. 7 [Cr/(Cr + Al)] of spinel as a function of the forsterite content of coexisting olivine. For explanation see text

conditions during the crystallization of the matrix ilmenite and ulvöspinel using the Fe-Ti oxide thermometer-oxybarometer (Spencer and Lindsley 1981; Anderson et al. 1991). Conditions of approximately 1200 °C and $\log f_{O2}$ of –9 have been obtained. The f_{O2} conditions correspond to NNO –1 log unit, a value typical for transitional basalts and OIB (e.g. Carmichael 1991; Ballhaus 1993). The high crystallization temperatures inferred from olivine-spinel and ilmenite-ulvöspinel thermometry are typical for basalt magmas with relatively low H_2O contents.

Bulk rock compositions

Analytical methods

Major-element determinations were performed by X-ray fluorescence after fusion with lithium tetraborate. Precision was typically better than ±1.5% for a concentration of 10 wt%. Zirconium was determined by X-ray fluorescence (XRF) on pressed pellets, with a precision better than ±4% at 100 ppm level. Trace-element determinations were done by inductively coupled plasma emission mass spectrometry (ICP-MS) after $HNO_3 + HF$ digestion of 100 mg sample powder in a Teflon-lined vessel at ~180 °C and ~14 bar during 30 min, evaporation to dryness, and subsequent dissolution in 100 ml of 4 vol% HNO_3. Instrument measurements were carried out in triplicate with a PE SCIEX ELAN-5000 spectrometer using Rb as internal standard. Precision was better than ±2 relative % and ±5 relative % for concentrations of 50 and 5 ppm, respectively.

$^{87}Sr/^{86}Sr$ and $^{143}Nd/^{144}Nd$ analyses were performed using a Finnigan MAT 262 RPQ spectrometer after separation by ion-exchange resins. External precision (2σ) measured in ten replicates of the standard WS-E (Govindaraju et al. 1994) was approximately ±0.003 relative % for $^{87}Sr/^{86}Sr$ and ±0.0026 relative % for $^{143}Nd/^{144}Nd$. $^{87}Rb/^{86}Sr$ and $^{147}Sm/^{144}Nd$ proportion were obtained by ICP-MS, with an external precision (2σ) better than ±1.2 relative % and ±0.8 relative %, respectively.

Selected samples

Most of the selected samples have only suffered moderate metamorphism, but a small number have been almost completely transformed during metamorphism with only occasional preservation of some relict igneous clinopyroxene. In all cases there is no visible deformation. Some of the non-metamorphic samples display hydrothermal alteration that produced albitization of the plagioclase phenocrysts in the porphyritic rocks that lead to formation of very-fine-grained aggregates in the matrix.

The metamorphosed igneous rocks are represented by remnants of omphacite + garnet ± zoisite/clinozoisite ± glaucophane ± paragonite eclogite assemblages that were largely replaced by barroisite + garnet + epidote + albite ± phengite (±paragonite) assemblages. Some samples display additional greenschist facies mineral assemblages. These rocks are not deformed and the metamorphism is believed to be related to the same alpine metamorphism of high-intermediate pressure and low temperature observed in the surrounding metasediments (Gómez-Pugnaire and Fernández-Soler 1987; Bakker et al. 1989; among others).

Major and trace element geochemistry

Despite the strong metamorphism of some specimens, all the metamorphosed samples show major-element chemical compositions that are essentially indistin-

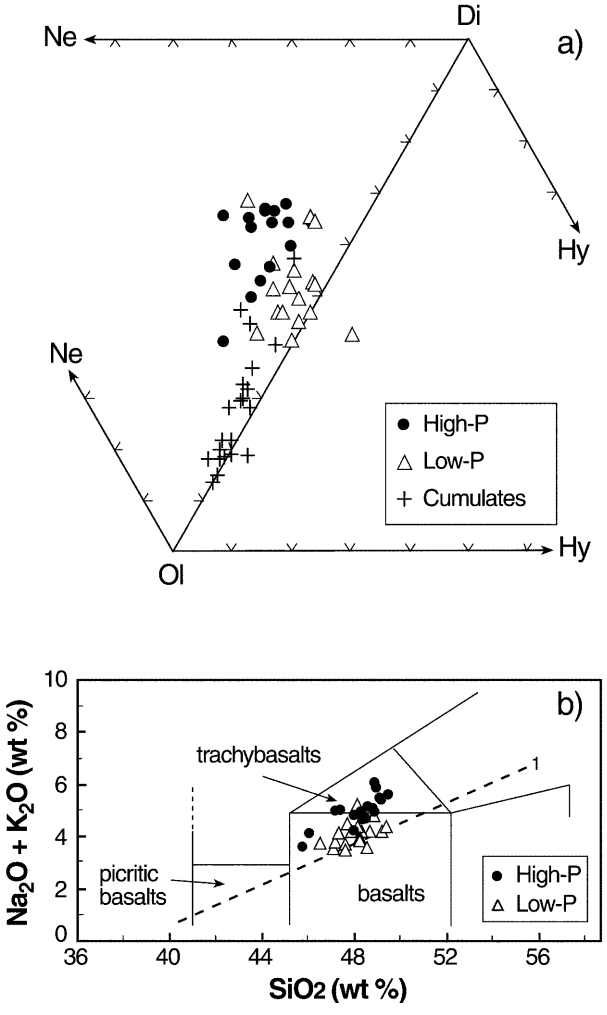

Fig. 8 **a** Normative classification diagram (after Yoder and Tilley 1962) of the Nevado-Filábride mafic rocks. Note the effect of the olivine accumulation and the higher degree of undersaturation of the samples from the high-*P* (Ti) basalts; **b** Total alkalis-silica (TAS) classification diagram for the basic rocks of the Nevado-Filábride Complex (after Le Bas et al. 1992). The broken line separating the alkaline and subalkaline series is taken from Irvine and Baragar (1971). The most alkaline compositions correspond to the high-*P* group

guishable from the unmetamorphosed samples. The Nevado-Filábride basic igneous rocks can be classified as alkaline basalts and basanites on the basis of their *normative* composition (Fig. 8a) (up to 17% Ne, assuming $Fe_2O_3/FeO = 0.15$, Table 2 and also Table 4 presented as electronic supplementary material) and the classification of Yoder and Tilley (1962). Only two samples (BM-1 and CC-12) with normative hypersthene (1.4–3.1%) correspond to olivine-tholeiites. In the classification diagram SiO_2 vs $Na_2O + K_2O$ (Fig. 8b; Le

Table 2 Major (wt%) and trace element (ppm) contents of selected samples of Nevado-Filábride mafic rocks. *PH* porphyritic sample; $X_{Mg} = [(Mg/Mg + Fe^{2+})]$ assuming $Fe_2O_3/FeO = 0.15$; *Ne, Di, Hy, Ol* CIPW-normative nepheline, diopside, hypersthene, and olivine

Sample rock type	CHE-1 dolerite[a]	CH-11 dolerite[a]	BM-1 gabbro	CC-3 gabbro	CEC-3 gabbro	CC-13 dolerite	CC-15 dolerite[a]	CC-18 dolerite[a]	CH-39 gabbro	CH-31a PH	CH-17 PH	CC-12 dolerite[a]	AL-16 dolerite[a]	CH-38 gabbro[a]	CH-49 gabbro[a]	CB-388 PH[a]
SiO_2	47.10	48.22	48.54	48.32	47.72	48.92	49.15	47.99	–	47.39	49.46	46.06	45.45	44.38	45.78	45.73
TiO_2	1.22	1.72	1.24	1.54	1.59	2.01	2.09	2.01	–	1.65	2.21	1.16	1.01	1.47	0.84	1.30
Al_2O_3	17.30	15.95	16.66	16.55	16.85	17.30	16.31	16.83	–	16.35	19.25	14.69	14.18	10.42	15.75	14.54
Fe_2O_3tot	11.72	11.60	11.74	10.67	10.28	8.53	9.29	10.06	–	9.99	8.42	11.36	11.67	12.70	11.02	10.94
MgO	8.37	9.14	8.05	8.84	9.31	7.96	8.21	7.54	–	10.00	5.24	15.70	17.00	21.65	15.12	14.10
MnO	0.18	0.15	0.16	0.15	0.14	0.07	0.15	0.10	–	0.08	0.08	0.16	0.16	0.20	0.17	0.16
CaO	10.49	9.23	9.91	9.37	9.38	8.86	8.97	10.33	–	9.30	9.41	7.88	7.57	6.36	8.41	9.86
Na_2O	2.97	3.44	3.12	3.54	3.77	5.44	3.94	4.22	–	4.28	5.07	2.45	2.43	2.17	2.60	2.95
K_2O	0.52	0.36	0.43	0.67	0.72	0.58	1.46	0.56	–	0.69	0.50	0.37	0.36	0.43	0.20	0.26
P_2O_5	0.12	0.18	0.15	0.17	0.24	0.32	0.43	0.37	–	0.28	0.36	0.17	0.16	0.22	0.10	0.17
Total	99.99	99.99	100.00	99.82	100.00	99.99	100.00	100.01	–	100.01	100.00	100.00	99.99	100.00	99.99	100.01
X_{Mg}	0.62	0.64	0.61	0.65	0.67	0.68	0.67	0.63	–	0.70	0.59	0.76	0.77	0.80	0.76	0.75
Ne	1.75	1.19	–	2.03	4.41	9.89	4.01	5.95	–	7.71	5.73	–	0.60	1.05	1.13	4.57
Li	9.9	5.3	15.9	17.9	30.4	26.6	25.8	7.2	–	75.9	46.6	8.0	42.9	10.5	4.3	29.3
Cs	0.8	0.2	0.4	0.6	0.7	0.7	1.6	0.3	–	1.4	0.8	0.4	1.6	0.7	0.6	2.8
Be	0.8	1.0	0.6	0.7	1.0	1.4	1.4	0.5	–	1.5	1.6	0.6	1.0	0.9	0.5	0.7
Rb	6.4	5.0	4.7	10.5	9.5	5.1	15.3	4.3	–	8.2	8.0	5.7	6.2	5.5	3.1	3.1
Sr	214.5	275.6	429.2	321.1	296.8	290.2	472.0	267.6	–	323.0	640.5	276.1	261.4	278.1	220.2	320.8
Ba	213.5	45.0	117.2	95.4	112.9	147.4	200.7	28.5	–	183.9	58.2	35.0	53.3	54.4	19.6	40.9
Sc	41.1	24.6	38.9	33.6	35.7	40.1	38.4	28.6	–	30.1	28.6	31.1	19.2	20.6	25.4	31.2
V	223.7	177.1	182.5	162.3	174.7	211.6	229.4	107.9	–	200.0	221.0	132.4	126.8	173.3	141.2	162.6
Cr	250.0	542.2	231.5	260.5	348.2	242.5	331.5	765.2	–	522.3	156.2	726.6	877.4	707.5	881.8	623.9
Co	69.3	65.5	70.8	64.5	77.2	74.3	77.6	92.3	–	48.1	66.6	105.0	85.0	91.9	82.8	79.7
Ni	143.0	224.0	141.9	169.7	202.0	129.9	174.0	505.0	–	232.4	64.5	451.0	477.0	581.0	423.0	456.0
Cu	100.0	85.1	131.5	29.1	60.5	30.0	84.6	102.3	–	10.6	16.1	103.5	84.9	59.9	88.5	81.3
Zn	75.4	96.8	164.4	122.4	147.6	98.8	181.5	124.4	–	33.1	17.5	166.0	70.6	103.2	78.3	69.3
Ga	16.2	17.8	16.5	17.1	17.2	17.8	18.2	13.2	–	17.4	20.6	14.4	13.7	12.6	13.7	13.1
Y	25.7	17.7	21.3	18.2	23.5	27.3	30.4	13.9	–	25.2	29.8	17.1	14.5	14.1	16.2	20.6
Nb	3.2	6.6	6.5	8.1	9.9	19.1	21.0	10.0	46.06	11.6	–	6.9	6.7	13.4	4.6	3.9
Ta	0.3	0.6	0.8	0.7	1.2	2.0	1.6	3.8	1.43	1.2	–	0.7	3.0	1.6	0.7	0.4
Zr	94.0	116.0	100.0	93.0	125.0	188.0	214.0	186.0	15.96	189.0	–	86.0	90.0	118.0	66.0	101.0
Hf	2.4	3.4	2.9	3.4	3.4	5.0	5.9	4.1	11.23	4.8	–	1.9	2.0	2.2	1.3	2.7
Mo	0.5	1.0	0.5	0.5	0.8	0.6	0.3	0.7	11.00	0.5	–	0.8	0.9	1.4	0.5	0.1
Sn	2.5	0.7	2.0	2.6	2.6	3.0	2.7	2.1	0.19	0.0	–	2.5	1.2	1.2	1.0	1.5
Tl	0.1	0.1	0.1	0.1	0.1	0.0	0.1	0.0	9.73	0.1	–	0.1	0.1	0.0	0.0	0.0
Pb	1.8	0.9	26.9	5.8	8.6	3.7	8.5	2.9	3.18	12.0	–	4.4	1.8	2.1	2.0	5.1
U	0.1	0.1	0.1	0.2	0.2	0.5	0.3	0.2	0.87	0.4	–	0.2	0.2	0.2	0.1	0.1
Th	0.6	0.4	0.5	0.6	0.9	1.3	0.9	0.6	0.36	1.1	–	0.7	0.6	0.4	0.3	0.3
La	4.6	5.4	5.9	6.5	8.8	14.0	16.9	5.3	100.01	12.0	–	6.3	6.8	6.5	2.7	4.3
Ce	12.3	13.3	15.6	16.1	22.7	36.4	41.9	13.3	0.69	28.3	–	16.1	14.8	15.2	6.8	11.4
Pr	1.8	1.9	2.3	2.2	3.2	4.6	5.5	1.9	5.36	3.8	–	2.2	1.8	2.1	1.0	1.7
Nd	8.5	9.2	10.6	10.7	14.9	22.0	25.1	8.8	62.6	16.1	–	10.5	8.1	9.1	4.7	8.6
Sm	2.7	3.0	3.1	3.2	4.0	5.4	6.1	2.4	1.9	4.1	–	2.8	2.1	2.4	1.4	2.6
Eu	1.0	1.1	0.9	0.9	1.1	1.3	1.5	0.7	1.3	1.4	–	0.8	0.8	0.9	0.6	1.0
Gd	3.5	3.6	3.6	3.7	4.2	5.1	6.1	2.5	13.9	4.5	–	2.9	2.4	3.0	2.1	3.1
Tb	0.6	0.6	0.6	0.6	0.7	0.7	1.0	0.4	447.3	0.8	–	0.5	0.4	0.5	0.4	0.6
Dy	4.2	3.2	3.9	3.6	4.3	5.1	5.9	2.6	213.1	4.3	–	3.1	2.5	2.7	2.6	3.7
Ho	1.0	0.7	0.8	0.7	0.9	1.0	1.1	0.5	24.3	0.9	–	0.7	0.5	0.5	0.6	0.8
Er	2.7	1.7	2.2	1.9	2.4	2.8	3.0	1.4	196.4	2.4	–	1.8	1.4	1.5	1.7	2.1
Tm	0.4	0.2	0.3	0.3	0.3	0.4	0.4	0.2	423.2	0.4	–	0.3	0.2	0.2	0.3	0.3
Yb	2.7	1.5	2.0	1.7	2.1	2.4	2.3	1.3	52.2	2.4	–	1.6	1.3	1.2	1.8	2.1
Lu	0.4	0.2	0.3	0.2	0.3	0.3	0.3	0.2	198.3	0.4	–	0.2	0.2	0.2	0.3	0.3
Di	15.0	14.0	14.4	14.5	14.3	16.5	15.3	18.8	12.4	16.3	–	8.0	7.6	9.9	8.1	17.3
Hy	0.0	0.0	3.1	0.0	0.0	0.0	0.0	0.0	59.7	0.0	–	1.4	0.0	0.0	0.0	0.0
Ol	19.0	20.0	16.5	18.9	19.1	13.9	15.5	13.8	15.8	18.8	–	33.4	36.6	44.2	32.7	27.1

[a] Samples without metamorphic overprint

Bas et al. 1992) the samples plot again in the fields of basalts and trachybasalts (hawaiites), near and above the subalkaline-alkaline line of Irvine and Baragar (1971). A good positive correlation between SiO_2 and total alkalis is observed; the correlation of Na_2O with SiO_2 is considerably better than that of K_2O (see Fig. 9e, f). The alkali contents are within the normal values for basalts. This suggests that the alkali content for most of these rocks was not dramatically modified by metamorphic or other post-magmatic process. Similarly Rb/Sr vs Rb/Nb and K_2O/Nb vs Rb/Nb relationships are characterized by good positive correlations suggesting that the alpine metamorphism did not seriously disturb the LILE vs HFSE relations of the basic igneous rocks (Fig. 11c, d).

The Ti/V ratios of 30–60 (Fig. 11f) is consistent with an alkaline to transitional magmatic affinity (Ti/V between 50 and 70) (Shervais 1982). Samples with lower Ti/V ratios in the order of 30–50 and hence with a more tholeiitic affinity are observed in unmetamorphosed and strongly metamorphosed specimens, irrespective of the lithological group. The negative trends for Ti (and V) versus MgO (Fig. 9b) and Mg-number [X_{Mg} = molar MgO/(MgO + FeO)] indicate that the rocks have not been affected by important Fe-Ti oxide and/or hornblende fractionation. The samples define linear trends with constant Ti/V (Fig. 11f) suggesting that differentiation of these magmas was dominated by olivine + plagioclase fractionation (Shervais 1982).

The studied basic rocks have Mg-numbers ranging from 0.56–0.80. The highest MgO contents (17.79–22.60 wt%) are exclusive to cumulates with coarse-grained gabbroic textures (hereafter referred as cumulate-gabbros). Some olivine-chromite-rich dolerites with MgO between 11 and 21 wt% are also cumulitic in origin. The variability of the Mg-number in the non-cumulitic samples is restricted (0.59–0.70). These rock samples do not define a good correlation between most major and minor elements and Mg-number. These results are supported by the small variability of the chemical composition of the main minerals. The apparent near-linear negative correlation between MgO and elements such as SiO_2, TiO_2, and Al_2O_3 (Fig. 9a, b, c) does not reflect the liquid line of descent of the magmatic suite investigated, but it results from the variable accumulation of olivine ± Cr-spinel. The linear correlation between MgO and Ni (Fig. 10a) is clearly indicative of olivine accumulation as opposed to a hy-

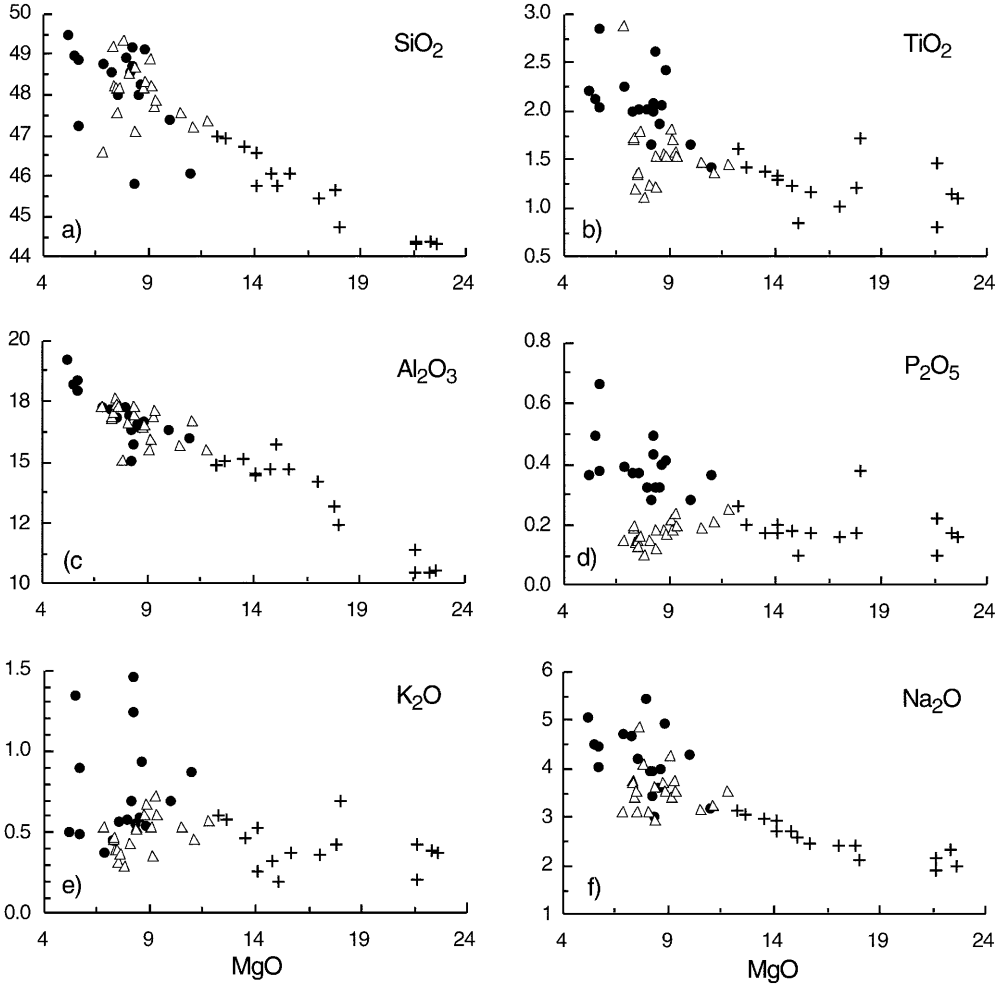

Fig. 9 Variation of major element oxides of the Nevado-Filábride mafic rock as a function of the MgO content. The effect of the olivine accumulation is clearly visible by the trend defined by the *crosses* (*filled circles* = high-phosphorous (Ti) rocks, *triangles* = low-phosphorous (Ti) rocks, *crosses* = cumulate rock samples)

perbolic trend produced by fractional crystallization (Hart and Davies 1978).

However, more detailed inspection of the MgO-variation diagrams reveals that the non-cumulitic samples (as defined by petrographic data) cover a range in composition for incompatible HFSE elements, Th and LREE that is best observed for P_2O_5, TiO_2, Nb, Zr, Th, La. (Figs. 9 and 10). The two distinct groups of basaltic rocks are also apparent in trace element ratio diagrams such as La/Yb vs MgO (Fig. 10h), Rb/Sr vs Rb/Nb (Fig. 11c), and in the Y vs Z diagram (Fig. 11b). In some diagrams, e.g. Rb/Sr vs Rb/Nb, the samples plot along two different lines or occupy distinct fields (e.g. Y vs Zr).

These contrasting geochemical features could stem from two different processes:

1. Fractional crystallization controlled by different mineral assemblages co-precipitating from a nearly identical parental alkaline to tholeiitic basaltic magma. Such a process would be supported by the rather peculiar differentiation trends of decreasing HFSE patterns with increasing differentiation (decreasing MgO and X_{Mg}). As opposed to most studies, where the HFSE content increases with differentiation (e.g. Sweeney et al. 1994) or form distinct groups over the entire differentiation interval, opposite trends starting from a 'common parent' around 10 wt% MgO are observed in the basaltic rocks of the Betic Cordillera. This feature is obvious when one compares the Zr/Y vs MgO diagram (Fig. 10f); Sweeney at al. (1994; their Fig. 12b observed separate groups at MgO-contents < 6 wt%, whereas in our Fig. 10f) we observe convergence at about $X_{Mg} = 0.7$, corresponding to a MgO-content of 9–10 wt%. The separation in two different groups can best be observed in the P_2O_5 vs MgO and TiO_2 vs MgO diagrams (Fig. 9b and d) and hereinafter they are called *low-P* and *high-P group*. The limiting concentration has arbitrarily been set at a P_2O_5 content of 0.25 wt% (see also Table 2). The decrease of HFSE in the low-*P* group demands the precipitation and fractionation of HFSE-rich minerals such as Fe-Ti-oxide (ilmenite), apatite, and zircon. This is not really supported by petrographic observation as all these accessory phases only occur in the matrix as relatively late precipitates.
2. An alternative explanation for temporally and spatially associated low- and high-*P* (and Ti) basaltic suites, not uncommon in continental basaltic provinces (e.g. Hawkesworth et al. 1983; Ellam and Cox 1991; Sweeney et al. 1994), is that they derive from different primary magmas. They may originate, respectively, from depleted MORB (mid-ocean ridge basalts)-type asthenospheric mantle sources and more enriched mantle sources incorporating metasomatically modified lithospheric components.

Trace element variation and ratio diagrams support the occurrence of two distinct magma types in the Nevado-Filábride basic igneous rocks: the V vs Ti (Fig. 11f), $(La/Yb)_N$ vs MgO (Fig. 10h), Zr vs Hf, Y vs Zr and Rb/Sr vs Rb/Nb (Fig. 11a–c) diagrams reveal a clear separation into two different groups. The Zr/Y vs Zr/Nb diagram often used to discriminate different potential mantle sources (Fig. 11e) shows considerable scatter with the low-*P* group trending versus N-MORB type values and the high-*P* group scattering versus an OIB-type mantle. Additionally, the samples show a tendency versus enriched mantle sources, possibly a metasomatized lithospheric component.

The REE diagrams (Fig. 12a, b, c) reflect the overall trend: samples from the low-*P* group have a generally flatter REE pattern and lower abundances of (chondrite normalized) LREE than the high-*P* group samples. The cumulate rocks have a variable REE distribution pattern; they reflect the variable proportions of cumulus phases and high- or low-*P* intercumulus liquid. The arrangement of the samples is not always according to their differentiation index: The low-*P* sample CHE-1 ($X_{Mg} = 0.61$) contains considerably lower LREE concentration than the less differentiated samples CC-3 or CEC-3 (Fig. 12a). In addition, the sample CHE-1 exhibits higher HREE contents than the other two samples resulting in a rotation of the REE pattern. Sample CHE-1 exhibits very low abundances of HFSE elements and plots closest to the N-MORB composition in the Zr/Y vs Zr/Nb diagram (Fig. 11e). Some of the spread observed in the REE diagrams is probably inherited from a variable mantle source (and possibly a variable degree of partial melting, see below) and does not result from differentiation. The high-*P* samples follow more closely a differentiation dominated trend of increasing $(La/Yb)_N$ with decreasing X_{Mg}, strongly inclined REE patterns [$(La/Yb)_N = 3$–5] and increasing overall REE abundances as expected in "normal" tholeiitic or alkaline differentiation. The sample CC-18 clearly falls out of the general trend: the relatively differentiated composition (xMg = 0.63) contrasts with its low REE abundance. The sample contains very high Cr, Co, and Ni content (770, 92, and 505 ppm) that indicate a considerable amount of accumulated olivine. CC-18 does not reflect a liquid composition but is rather a cumulate with highly differentiated intercumulus liquid.

The HREE contents of both, high- and low-*P* samples are lower than that of E-MORB basalts and OIB basalts (Sun and McDonough 1989; McKenzie and O'Nions 1995) probably reflecting the presence of garnet in the source during partial melting. La/Nb ratios consistently < 1 (Table 4) can be produced by relatively low

Fig. 10 Variation of selected minor and trace elements of the Nevado-Filábride mafic rock as a function of the MgO content. Linear arrays in the Ni and Cr diagrams are indicative of olivine + chromite ± clinopyroxene accumulation. The separation in two different groups (low-*P* and high-*P* basaltic rocks) is evident in the Zr, Nb, Th, and La diagrams. **h** Normalized (La/Yb) ratio vs MgO (normalization values were taken from Sun and McDonough 1989). See text for further explanation. Symbols as in Fig. 9

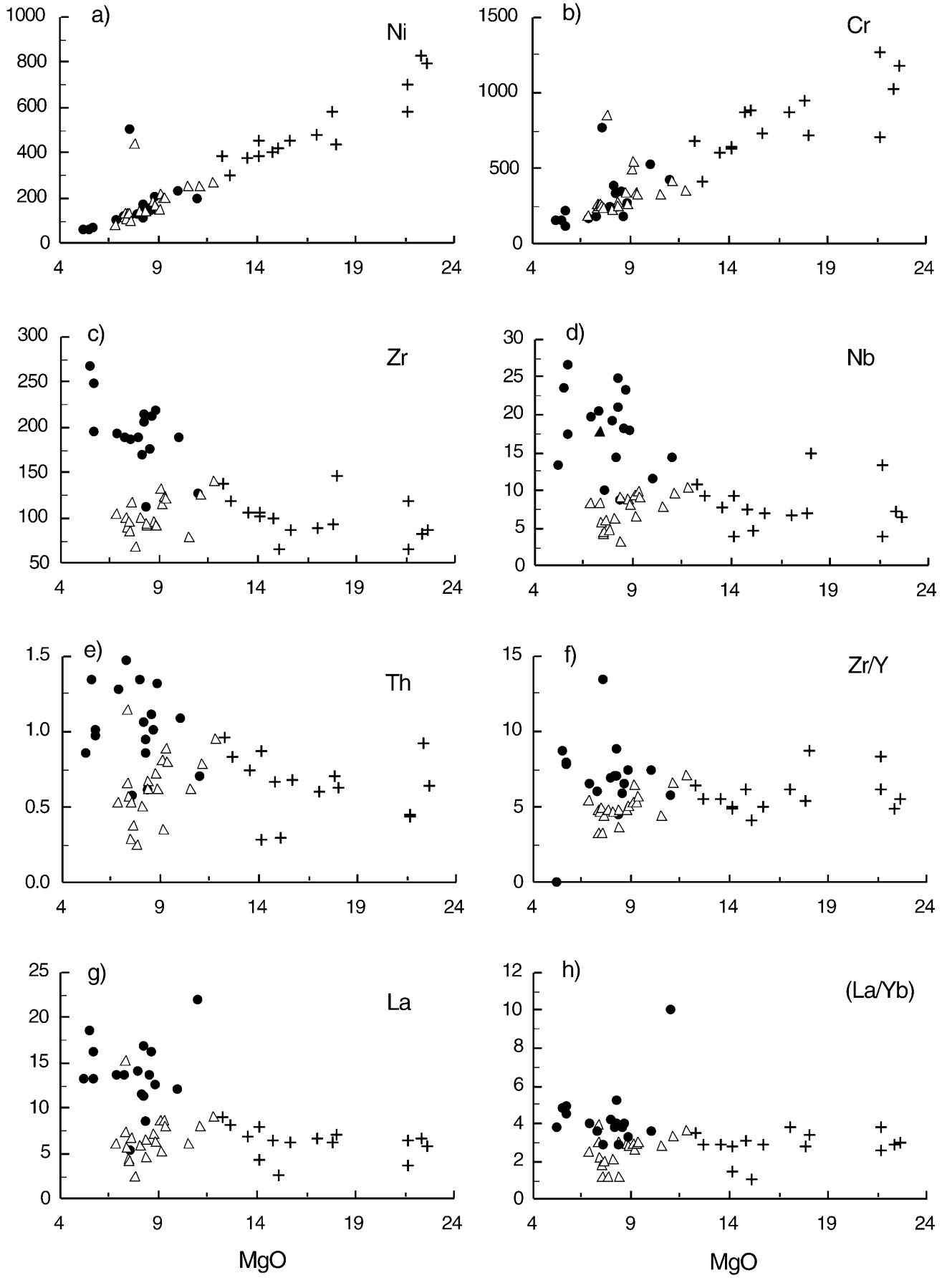
a)
Ni
b)
Cr
c)
Zr
d)
Nb
e)
Th
f)
Zr/Y
g)
La
h)
(La/Yb)
MgO
MgO

degrees of partial fusion from a garnet-bearing source and it is consistent with the LREE enrichment.

The trace element variations diagrams (Fig. 13a, b, c) confirm the observations made for the REE pattern and are in agreement with the general observation that the investigated igneous rocks most probably form part of a continental igneous suite resembling continental basalts erupted in rift zones and flood basalt provinces (e.g. Hergt et al. 1991; McKenzie and O'Nions, 1995). The overall trace element variation shows a modest increase from the compatible to moderately incompatible elements to the highly incompatible LREE elements. Alkaline elements and Ba show a wide range of scatter (see patterns displaying negative and positive Ba anomaly in Fig. 13) probably related to subsolidus alteration and metamorphic overprint.

Sr-Nd isotope geochemistry

Sr and Nd isotopes have been measured on a variety of samples from cumulitic and non-cumulitic rocks, fresh and strongly overprinted specimens, and low- and high-*P* basalts. The analytical results are given in Table 3 and presented in Fig. 14. εNd (Fig. 14a) varies within a very restricted range of 7.66 to 8.62 with one exception (CH-34, εNd + 6.52) that might be the result of crustal contamination. Sr is raised from $^{87}Sr/^{86}Sr = 0.7026$ to 0.7061. Such a horizontal shift of $^{87}Sr/^{86}Sr$ in the εNd vs εSr diagram results most probably from carbonate contamination during emplacement or subsequent metamorphism. The $^{87}Sr/^{86}Sr$ vs 1/Sr diagram (Fig. 14b) reveals that the increase of εSr negatively correlates with 1/Sr. This is the inverse of the pattern normally observed for contamination with granitic contaminants of continental origin that exhibit low Sr (high 1/Sr) abundance. The contaminant has high $^{87}Sr/^{86}Sr$ and high Sr abundances, but very low Nd abundances as the Nd isotopes are not affected at all. Carbonates (or seawater) have these geochemical characteristics. The sample CH-34, which plots off the general trend in Fig. 14a, has rather low Sr-content, but nevertheless shows increased εSr accompanied by low εNd. This sample, as an exception, might have suffered crustal contamination. The uncontaminated samples (CB 41/12, CH-49, CC-12, and CH-11) define a restricted area in εNd – εSr space, which coincides with the most depleted values observed for PREMA (prevalent mantle; Zindler and Hart 1986), typical for continental basalts and OIB, but less depleted than present-day MORB. The observed compositions are consistent with a time-integrated, depleted, and subcontinental lithospheric mantle source that suffered variable degrees of metasomatic incompatible element enrichment. Such isotopic relationships are often observed in continental and oceanic alkaline and transitional basalt associated with a crustal extension lacking evidence for a plume-related mantle source (e.g. McKenzie and O'Nions 1995).

Characterization of the mantle sources

REE abundances and the shape of the REE distribution patterns have been used to characterize the potential mantle source and to constrain the amount of partial melting that lead to the formation of the primary basaltic magmas (such as CH-31A).

Batch melting calculations have been performed assuming a primitive mantle source with chondrite normalized $(La/Yb)_{CN} = 1.000$ and $(Yb)_{CN} = 2.900$ (Sun and McDonough 1989) and a variety of peridotite residua varying from garnet lherzolite to garnet (-spinel)-free lherzolite, with melting percentages up to 50% (Fig. 15). The results indicate that the near primary rocks investigated in this study could have been produced by approximately 5–12% melting from a garnet-bearing (maximum 2%) lherzolite. These results are consistent with the observed REE-patterns, the low values of the $(La/Nb)_{PM}$ (mean 0.88 $\pm$ 0.22, range 0.48–1.58; Thompson and Morrison 1988), and the high Nd and low Sr isotopic compositions, pointing towards a previously depleted subcontinental lithospheric mantle. The low-*P* (and Ti) basalts correspond to the higher degree (8–12%) melting with respect to the high-*P* (and Ti) basalts (5–8%). The results are consistent with recent partial melting experiments on dry, fertile (MORB-pyrolite) spinel and garnet-bearing peridotites (e.g. Falloon et al. 1988; Robinson and Wood 1998): Up to 14% partial melting nepheline-normative basaltic melts are produced. Only at higher melting percentages do the partial melts become enstatite-normative.

Discussion and conclusions

The Nevado-Filábride metabasites, their geochemical character, and the tectonic setting in which they intruded are the subject of an ongoing extensive discussion. Origins proposed for these rocks can be grouped essentially in two main hypotheses: (1) they formed during a continental rifting stage (Vegas and Muñoz 1986; Muñoz 1986; Franz et al. 1988; Gómez-Pugnaire and Muñoz 1991) or (2) they originated as dismembered parts of oceanic crust (Bodinier et al. 1987; Puga et al. 1989). Obviously, these hypotheses have different implications concerning the pre-metamorphic scenario of the Betic complex.

This controversy on the magmatic history of the Nevado-Filábride metabasites originates from the following facts: (1) basic igneous rocks constitute only a very small percentage of the total volume of the Nevado-Filábride materials and they always appear as discontinuous and strongly deformed bodies; (2) the metabasites, as well as the metasediments, underwent a high grade metamorphic overprint that obliterated most of the igneous features, and the pre-metamorphic relationships between the lithologies; (3) the geochemical affinity of the magmatism is ambiguous, because it can occur in both oceanic and continental settings; (4) the

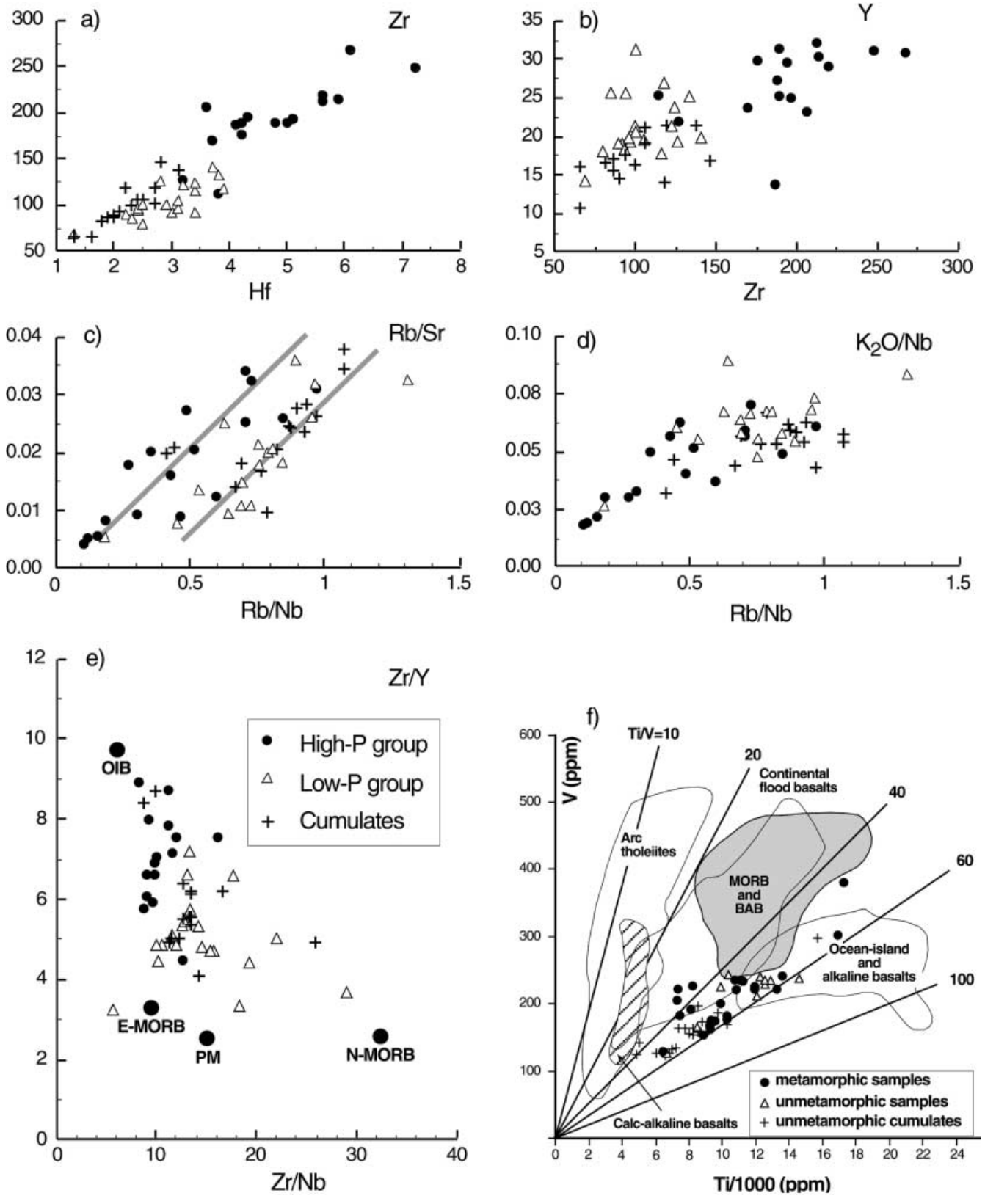

Fig. 11a–f Incompatible element and ratio variation diagrams of the Nevado-Filábride mafic rock. **a** Zr vs Hf; **b** Y vs Zr; **c** Rb/Sr vs Rb/Nb, low- and high-*P* (Ti) group samples align along two distinct trends; **d** K_2O/Nb vs Rb/Nb; **e** Zr/Y vs Zr/Nb, the values for OIB, PM, E- and N-MORB are taken from Sun and McDonough (1989); **f** Ti vs V variation diagram showing the fields for rocks originating from different geological settings. Lines of constant Ti/V ratios are given for reference. Most of the Nevado-Filábride samples have Ti/V ratios between 40 and 60 that correspond to alkaline (35–75) and transitional (30–50) basalts

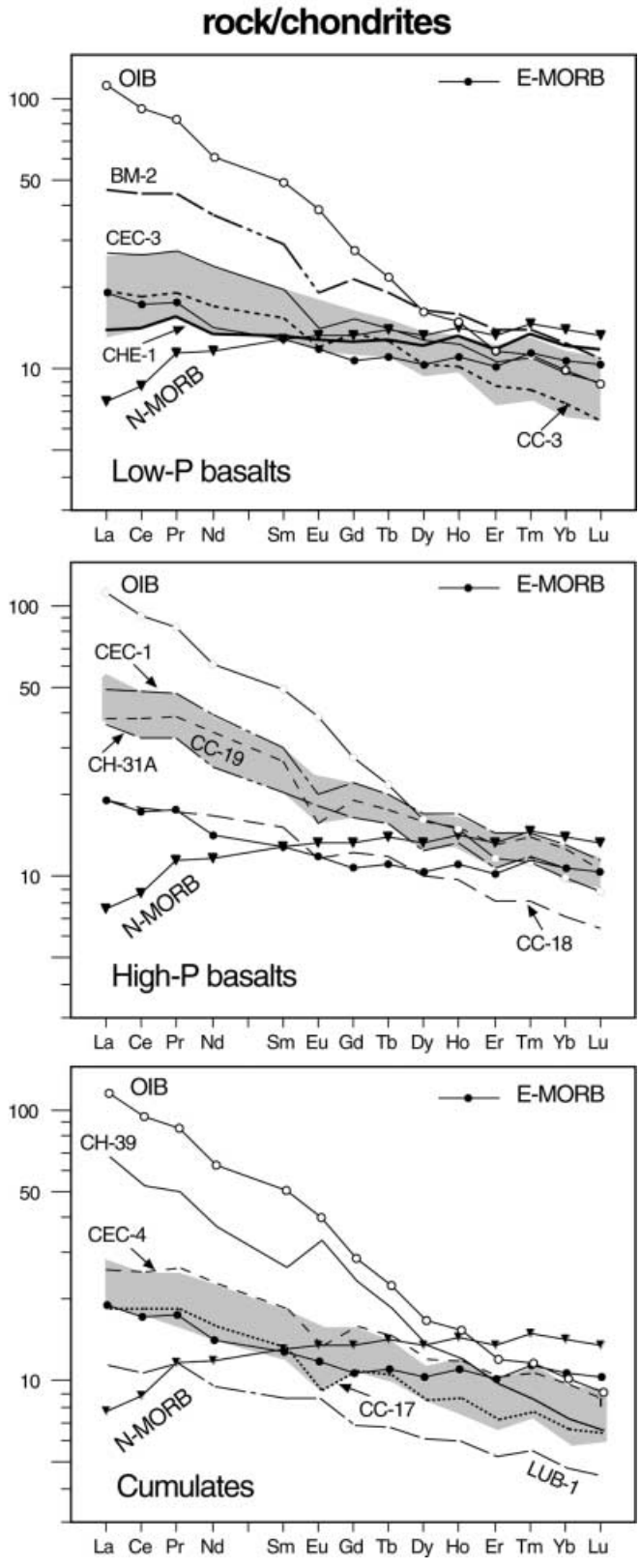

Fig. 12 Chondrite-normalized REE patterns for the samples of the Nevado-Filábride mafic rocks. *Shaded areas* indicate the REE variation of all samples of a particular group (low-*P* basalts, high-*P* basalts, cumulate rocks). The most significant samples and samples plotting outside the *shaded areas* are reported separately. The normalization values and the REE-patterns for OIB, E- and N-MORB given for comparison are taken from Sun and McDonough (1989)

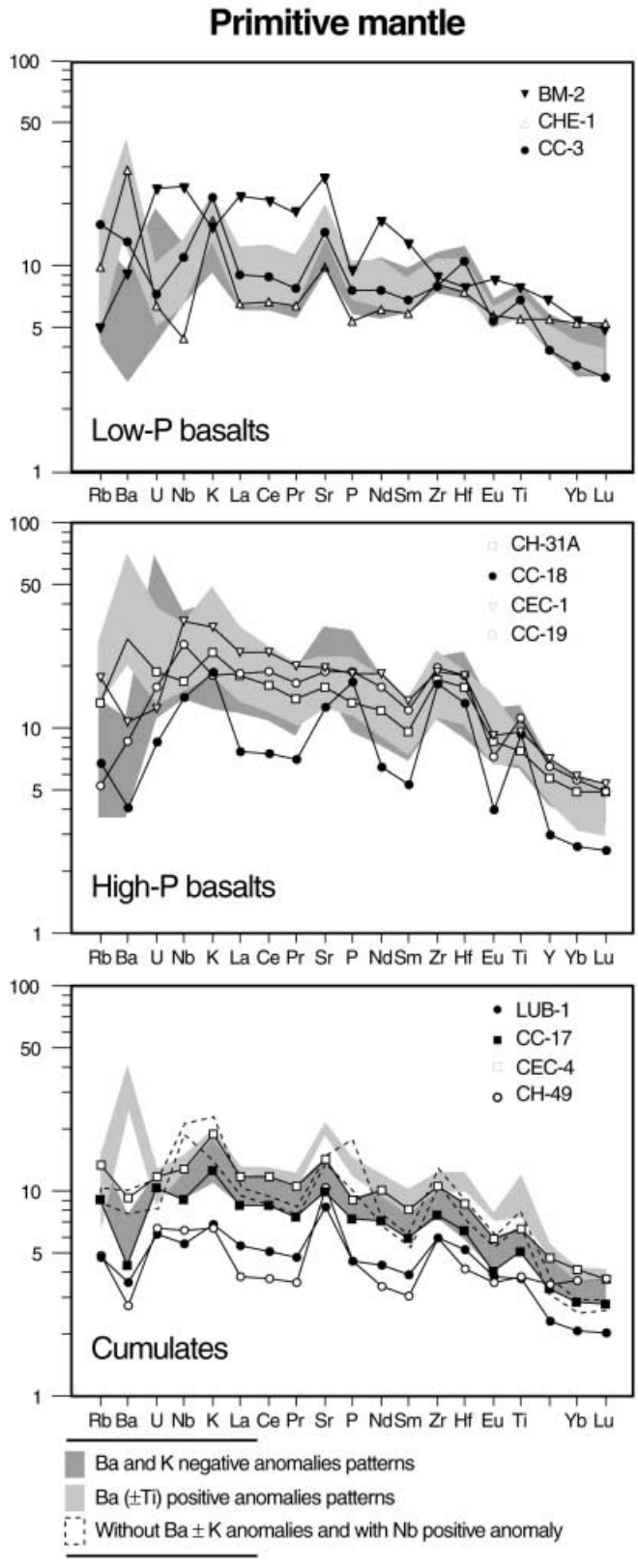

Fig. 13 Primitive mantle-normalized trace element variation diagrams for representative Nevado-Filábride mafic rocks. Most of the sample plot in the *shaded* and *outlined areas*. The most significant samples and samples plotting outside the *shaded areas* are reported separately. Normalization values are taken from Sun and McDonough (1989). The trace element patterns for OIB, E- and N-MORB are shown for comparison. For discussion see text

Table 3 Sr and Nd isotope data for selected samples of the Nevado-Filábride mafic rocks. *PH* Porphyritic sample; Rb, Sr, Sm and Nd contents measured by isotopic dilution; $^{87}Sr/^{86}Sr$, $^{143}Nd/^{144}Nd$ are present day values; εSr_{150} and εNd_{150} are calculated assuming an age of 150 Ma

Sample	Rock	Rb ppm	Sr ppm	$^{87}Rb/^{86}Sr$	$^{87}Sr/^{86}Sr$	Sm ppm	Nd ppm	$^{147}Sm/^{144}Nd$	$^{143}Nd/^{144}Nd$	εSr_{150}	εNd_{150}
CB-41/12[a]	dolerite	7.9	267.7	0.085	0.70268	2.53	9.31	0.1640	0.51303	−25.7	8.2
CC-12[a]	dolerite	2.9	256.5	0.032	0.70269	2.33	8.68	0.1626	0.51303	−24.0	8.2
CC-15[a]	dolerite	14.1	453.7	0.090	0.70379	4.87	19.69	0.1497	0.51303	−10.0	8.5
CC-19	dolerite	3.3	386.9	0.025	0.70530	4.54	17.94	0.1529	0.51302	13.4	8.4
CH-11[a]	dolerite	7.7	278.5	0.080	0.70266	3.01	9.73	0.1872	0.51305	−25.8	8.2
CH-34[a]	dolerite	5.6	203.3	0.080	0.70340	2.59	7.78	0.2015	0.51298	−15.3	6.5
CH-41[a]	dolerite	11.2	451.4	0.072	0.70417	4.10	15.81	0.1567	0.51301	−4.1	7.9
CC-11	gabbro	4.0	324.6	0.036	0.70369	3.10	10.80	0.1736	0.51301	−9.9	7.7
CH-49[a]	gabbro	3.2	201.7	0.046	0.70266	1.79	5.95	0.1817	0.51302	−24.9	7.8
CH-40	PH	5.5	707.3	0.022	0.70612	7.18	28.95	0.1499	0.51303	25.0	8.6

[a] Samples without metamorphic overprint

limited number of radiometric ages for the metabasites; and (5) the appearance of rodingitized dikes of basic rocks crosscutting the largest ultramafic bodies of the complex, which has been used to infer an ophiolitic sequence. Nevertheless, there are sufficient field and geochemical data to support alternative interpretations.

In the following discussion we propose that the origin and tectonic setting of the basic magmatism of the NFC is consistent with the rifting hypothesis outlined above. This interpretation is based on (1) the character of the sedimentary sequence in which the basic rocks intruded; (2) the field relationships between sediments and igneous rocks in the Cóbdar area; and (3) the geochemical constraints presented previously.

The shallow-marine character of the sediments

All sedimentary formations (Fig. 2) of the Cóbdar area preserve sedimentary and mineralogical features consistent with shallow-marine to epicontinental depositional

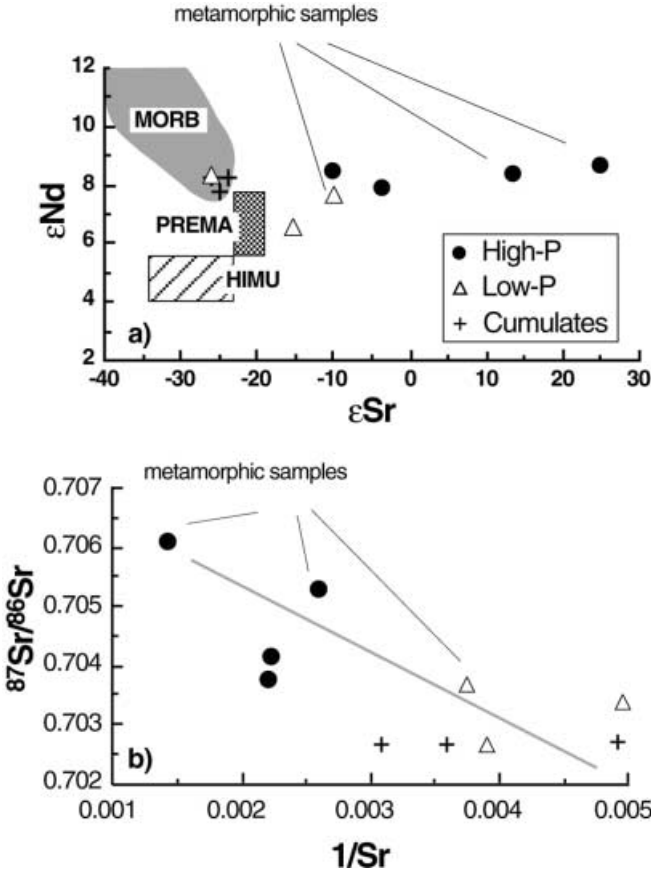

Fig. 14 **a** εSr vs εNd isotope diagram of the Nevado-Filábride mafic igneous rocks. The mantle components (PREMA, HIMU, and MORB) are taken from Zindler and Hart (1986); **b** Plot of $^{87}Sr/^{86}Sr$ ratios versus the reciprocals of the strontium concentration. For explanation see text

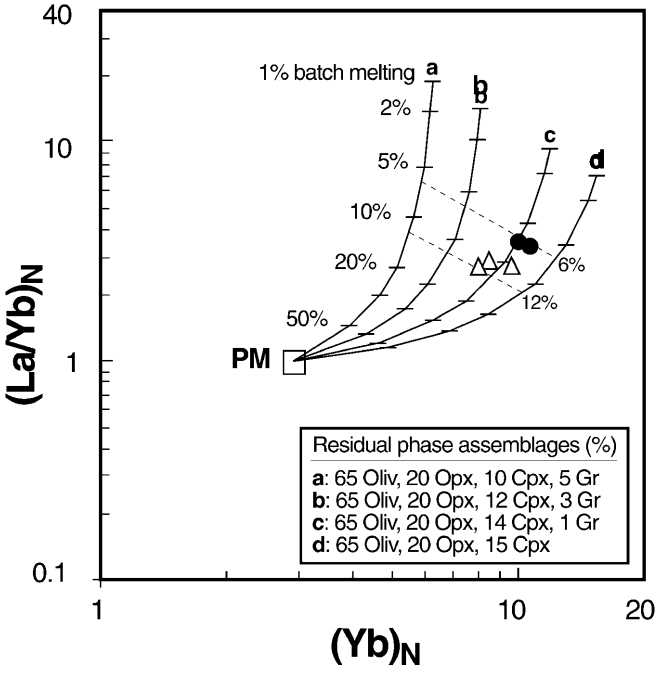

Fig. 15 Chondrite normalized $(La/Yb)_N$ vs $(Yb)_N$ diagram showing the composition of primary liquids generated by various degrees of batch melting of a starting composition (PM) with $(La/Yb)_N = 0.9996$ and $(Yb)_N = 2.9000$ that corresponds to the primitive mantle of Sun and McDonough (1989). Each *curve* represents a different residual mineral assemblage. The envelopes of 6% and 12% melting shown by *dashed lines* include the representative points of primitive samples of the low-*P* (Ti) basalts (*triangles*) and high-*P* (Ti) basalts (*filled dots*). The partition coefficients used for the batch melting calculations are from Rollinson (1995)

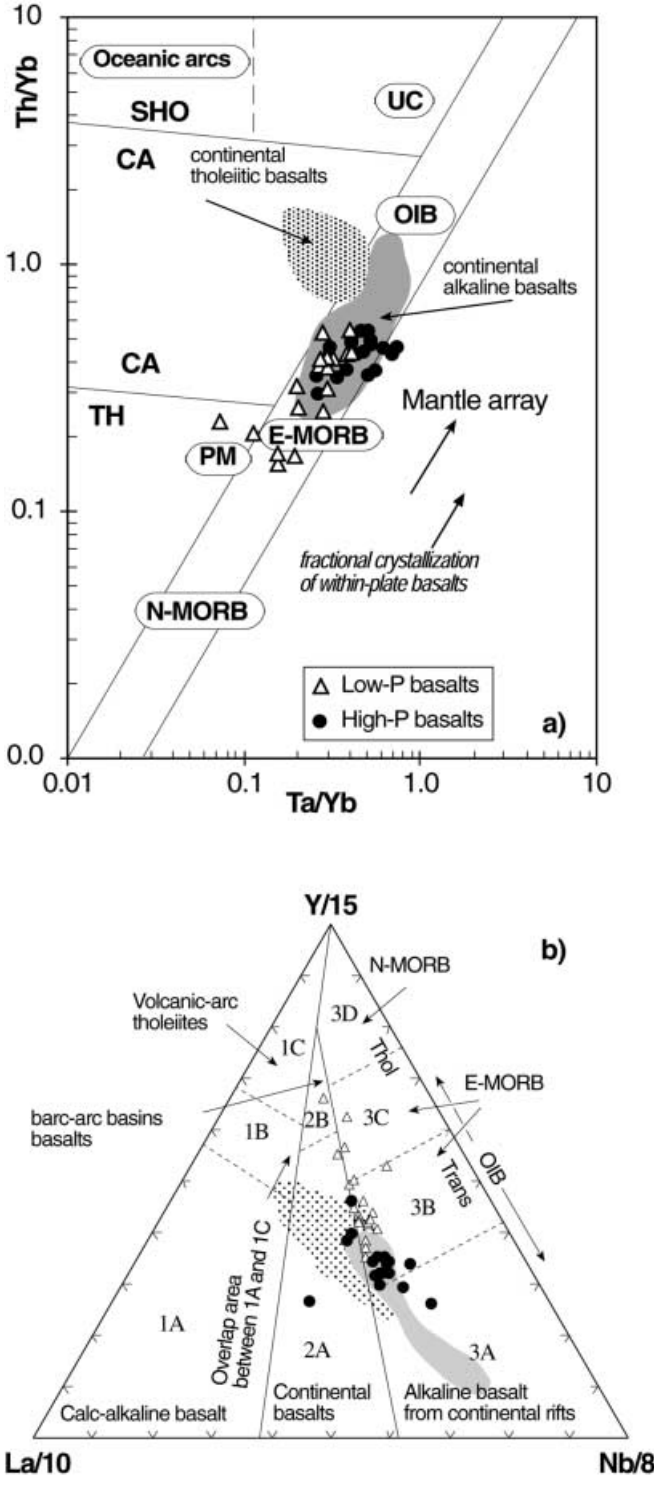

Fig. 16 **a** Th/Yb vs Ta/Yb diagram after Pearce (1982). Most samples from the Nevado-Filábride Complex are compatible with an origin from a within-plate geological setting. Some of the more evolved low-*P* (Ti) samples display the strongest tholeiitic affinity (after Pearce 1982). *CA* calc-alkaline series; *SHO* shoshonitic series; *TH* tholeiitic series; *PM*, primitive mantle; *UC*, average composition of the upper continental crust. OIB, E-MORB, and N-MORB values are taken from Sun and McDonough (1989); **b** Y – La – Nb discrimination diagram (from Cabanis and Lecolle, 1989) that displays the alkaline and transitional character of the majority of the samples of the mafic rocks with a small number of low-*P* (Ti) samples that display a pronounced tholeiitic affinity. Continental alkaline basalts (*shaded area*) and tholeiitic basalts (*stippled area*) from the external zones of the Betic Cordilleras (Morata et al. 1997) are given for comparison

environment of the Nevado-Filábride metasediments. Typical sedimentary structures of shallow-marine siliciclastic platforms, such as pervasive metric-scale trough cross-bedding, cm-scale ripples, and bioturbation are frequently observable in the quartzites of the *Tahal formation* (De Jong and Bakker 1991, Gómez-Pugnaire et al. 2000). The evaporitic origin of the MEV formation is attested by the presence of abundant gypsum pseudomorphs, Cl-rich scapolite, tourmaline, halite, sylvite, anhydrite and barite (Gómez-Pugnaire et al. 1994). The laminate marbles at the top of the cover sequence are probably peritidal in origin, although continental settings cannot be excluded (Gómez-Pugnaire et al. 2000). López-Sánchez-Vizcaíno et al. (1995) have inferred a coastal origin for the chomite-bearing calcareous intercalations. The sedimentary environment described for the Cóbdar area is comparable to many other geological sections of the NFC (Nijhuis 1964; De Jong and Bakker 1991; Jabaloy 1993; Soto 1993, Muñoz 1986). The change from shallow-marine quartzites to the overlying metaevaporites and coastal Cr-bearing marbles can only be the result of a regression from platform to coastal to continental environments.

The nature of the original mafic-wall rocks' contacts

The largest and best-exposed bodies of the Nevado-Filábride basic rocks are those of the Cóbdar area, where they occur as multiple and composite sill and dike intrusive bodies. Sharp intrusive contacts, chilled margins and apophyses in the metasediments (Nijhuis 1964; Muñoz 1986; Franz et al. 1988; De Jong and Bakker 1991) characterize their relationships with the shallow marine metasediments. The lack of basic igneous rocks in the studied area that preserve unequivocal features attributable to extrusive facies confirms the essentially intrusive or subvolcanic character of this magmatism. Nevertheless, a layer of extrusive submarine rocks, overlaying this intrusive group, has been proposed (Puga et al. 1989) on the basis of: (1) the interpretation of some rounded fragments of post-metamorphic brecciated porphyritic dikes as pillow-lavas (Puga et al. 1989); and (2) the occurrence of two isolated very small bodies (300×500 m) of basic rocks that resemble volcanic lavas (Puga et al. 1995; Cámara 1995). It should be noted, however, that it has not been demonstrated that these basic rocks are part of the same magmatism investigated in the present study (these bodies occur in the Lugros area, 100 km to the west, see Fig. 1).

The above sedimentary and tectonic relationships depict reasonably well a continental tectonic scenario for the Nevado-Filábride basic magmatism. The magma generation and emplacement took place in a continental rift zone, developed in Triassic to Jurassic times (De Jong

Table 4 Geological setting of the Nevado-Filábride mafic rocks deduced from referred discrimination diagrams

Reference	Diagram	Geological setting
Pearce and Cann (1973)	Ti-Zr-Y	Within-plate alkaline and tholeiitic basalts
Wood (1980)	Hf-Th-Ta	Within-plate tholeiitic (overlap with E-MORB) and alkaline basalts
Shervais (1982)	Ti-V	Continental alkaline and tholeiitic basalts
Pearce (1982)	Th/Yb Ta/Yb	Most are within-plate basalts and some samples are E-MORB
Meschede (1986)	Nb-Zr-Y	Within-plate alkaline and tholeiitic basalts
Cabanis and Lecolle (1989)	Y-La-Nb	Alkaline basalts in continental rifts, E-MORB
Cabanis and Thiéblemont (1988)	Tb-Th-Ta	continental basalts

1991), with the subsequent tectonic thinning of the crust. The continental setting is strongly supported by the occurrence of crustal xenoliths in the basic rocks (Gómez-Pugnaire and Muñoz 1991).

Geochemistry and tectonic setting

The tectono-magmatic diagrams (Fig. 16 and Table 4) indicate alkaline and minor tholeiitic affinities and a within-plate environment for the analyzed rocks, except in Cabanis and Thiéblemont's (1988) and Cabanis and Lecolle's (1989) diagrams. In their diagrams most of the samples plot in the enriched E-type MORB field or in the limits with the continental basalts. The slight but systematic geochemical differences between the low-*P* (Ti) and high-*P* (Ti) samples are evident in the diagrams of Figs. 9 to 11. These differences can be accounted for if the high-*P* basalts originated from batch melting of a more incompatible element-enriched source (OIB-type) than that of the low-*P* basalts (E-MORB-type). A variation of the amount of partial melting alone, as suggested by batch melting calculations (Fig. 15) cannot account for the observed spread in the geochemical and isotope (Fig. 14) data. The REE patterns and trace element variation diagrams (Figs. 12,13) display the enrichment in highly incompatible elements expected for magmas derived from mantle sources more enriched than E-type MORB, although not as greatly enriched as the OIB sources (Sun and McDonough 1989; Pearce and Parkinson 1993). These diagrams suggest, additionally, that partial melting possibly occurred in the stability field of garnet (McKenzie and O'Nions 1995).

The geochemical features of this magmatism suggest an evolution in two main stages during the progressive extension of the continental crust. In the early rift stage, small volumes of more alkaline magmas were generated, followed by the production of alkaline-transitional melts during the major rift stage (crustal thinning). It should be noted, however, that voluminous tholeiitic magmatism is missing, which typically precedes continental separation (e.g. Karoo, Paraná, Central Atlantic Magmatic Province, Ethiopia-Yemen) and the formation of the early oceanic crust. A potential link of the alkaline to transitional Nevado-Filábride basic magmatism with the voluminous, more tholeiitic Central Atlantic Magmatic Province (CAMP) that is associated with the breakup of Pangea at the Triassic-Jurassic boundary (e.g. Marzoli et al. 1999) cannot be determined unequivocally to date. The CAMP magmas intruded in a narrow time window of 190–200 my (Marzoli et al. 1999). The limited age data available on the Nevado-Filábride basic magmatism indicate ages of 140–180 my, considerably younger than the CAMP. If the Nevado-Filábride basic magmatism represents indeed a late expression of extensional tectonics related to the breakup of Pangea and the opening of the Atlantic Ocean in Triassic to Jurassic time remains speculative to date.

Acknowledgements We thank J.M. Fernández for his comments on an earlier version of this paper. Valuable discussions with Othmar Müntener during various stages of this project contributed to the final version. A very thorough, critical review by Enzo M. Piccirillo and critical comments by Michael Dungan are gratefully acknowledged; they helped improve the manuscript. We are also very grateful to F. Bea and P. Montero for their help and advice with the isotope analyses. This work was supported by the RNM-0145 Junta de Andalucia research group and by the DGICYT Project PB95–1266.

References

Aldaya F, Alvarez F, Galindo-Zaldívar J, González-Lodeiro J, Jabaloy A, Navarro-Vila F (1991) The Malaguide-Alpujarride contact (Betic Cordilleras, Spain) a brittle extensional detachment. C R Acad Sci, Ser II 313: 1447–1453

Anderson DJ, Bishop FC, Lindsley DH (1991) Internally consistent solution models for Fe-Mg-Mn-Ti oxides; Fe-Mg-Ti oxides and olivine. Am Mineral 76: 427–444

Azambre B, Rossy M, Albarède F (1992) Petrology of the alkaline magmatism from the Cretaceous North-Pyrenean rift zone (France and Spain). Eur J Mineral 4: 813–834

Bakker HE, De Jong K, Helmers HC (1989) The geodynamic evolution of the internal zone of the Betic Cordilleras, (southeast Spain). A model based on structural analysis and geothermobarometry. J Met Geol 7: 359–381

Ballhaus CH (1993) Redox state of lithospheric and asthenospheric upper mantle. Contrib Mineral Petrol 114: 331–348

Bodinier JL, Morten L, Puga E, Díaz de Federico A (1987) Geochemistry of metabasites from the Nevado-Filábride Complex. Betic Cordilleras, Spain: relics of a dismembered ophiolitic sequence. Lithos 20: 235–245

Cabanis B, Lecolle M (1989) Le diagramme La/10-Y/15-Nb/*: un outil pour la discrimination des series volcaniques et la mise en evidence des processus de melange et/ou de contamination crustale. CR Acad Sci, Ser II 309: 2023–2029

Cabanis B, Thiéblemont D (1988) La discrimination des tholéiites continentales et des basaltes arrière-arc. Proposition dun nouveau diagramme, le triangle Th3-Tb2-Ta. Bull Soc Geol France 4: 927–936

Cámara F (1995) Estudio cristalquímico de minerales metamórficos en rocas básicas del Complejo Nevado-Filábride (Cordilleras Béticas). PhD Thesis, University of Granada

Carmichael ISE (1991) The redox states of basic and silicic magmas: a reflection of their source regions? Contrib Mineral Petrol 106: 129–141

Comas MC, García-Dueñas V, Jurado MJ (1992) Neogene tectonic evolution of the Alboran basin from MCS data. Geo Marine Letters 12: 157–164

De Jong K (1991) Tectono-metamorphic studies and Radiometric dating in the Betic Cordilleras (SE Spain), with implications for the dynamics of extension and compression in the western Mediterranean area, PhD Thesis, University of Amsterdam

De Jong K, Bakker HE (1991) The Mulhacén and Alpujárride Complex in the Sierra de los Filabres, SE Spain: lithostratigraphy. Geol Mijnbouw 70: 93–103

Dobosi G (1989) Clinopyroxene zoning patterns in the young alkali basalts of Hungary and their petrogenetic significance. Contrib Mineral Petrol 101: 112–121

Duda A, Schmincke HU (1985) Polybaric differentiation of alkali basaltic magmas: evidence from green-core clinopyroxenes (Eifel, FRG). Contrib Mineral Petrol 91: 340–353

Egeler CG (1963) On the tectonics of the eastern Betic Cordilleras (SE Spain). Geol Rundsch 53: 260–269

Ellam RM, Cox KG (1991) An interpretation of Karoo continental flood basalts in term of interaction between asthenospheric magmas and the mantle lithosphere. Earth Planet Sci Lett 105: 230–242

Engi M (1983) Equilibria involving Al-Cr spinel: Mg-Fe exchange with olivine. Experiments, thermodynamic analysis, and consequences for geothermometry. Am J Sci 283 A (Orville Volume): 29–71

Falloon TJ, Green DH, Hatton CJ, Harris KL (1988) Anhydrous partial melting of a fertile and depleted peridotite from 2 to 30 kb and application to basalt petrogenesis. J Petrol 29: 1257–1282

Franz G, Gómez-Pugnaire MT, Muñoz M (1988) Mise en évidence d'une nouvelle étape de métamorphisme dans les dykes basiques des zones de Lubr'in et Cóbdar (Cordillères Bétiques, Nevado-Filábrides, Espagne). CR Acad Sci Paris, Série II 307: 2042–2047

Fujii T (1977) Fe-Mg partitioning between olivine and spinel. Carnegie Inst Wash Yb 76: 563–569

Galindo-Zaldívar J (1993) Geometría de las deformaciones neógenas en Sierra Nevada (Cordilleras Béticas). PhD Thesis, University of Granada

Galindo-Zaldívar J, González-Lodeiro F, Jabaloy A (1989) Progressive extensional shear structures in a detachment contact in the western Sierra Nevada (Betic cordilleras, Spain), Geodin Acta 3: 73–85

García-Dueñas V, Martínez-Martínez JM, Orozco M, Soto JI (1988) Plis-nappes cisaillements ductiles-fragiles en distension dens les Nevado-Filábrides (Cordillères Bétiques, Espagne). CR Acad Sci Paris, Ser II 307: 1389–1395

Gómez-Pugnaire MT (1981) La evolución del metamorfismo Alpino en el Complejo Nevado-Filábride de la Sierra de Baza (Cordilleras Béticas, España). Tecniterrae, pp 1–130

Gómez-Pugnaire MT, Fernández-Soler JM (1987) High-pressure metamorphism in metabasites from the Betic Cordilleras (SE Spain) and its evolution during the Alpine orogen. Contrib Mineral Petrol 95: 231–234

Gómez-Pugnaire MT, Muñoz M (1991) Al-rich xenoliths in the Nevado-Filábride metabasites: evidence for a continental setting of this basic magmatism in the Betic Cordilleras (SE Spain). Eur J Mineral 3: 193–198

Gómez-Pugnaire MT, Fontboté JM, Sassi FP (1982) On the occurrence of a metaconglomerate in the Sierra de Baza (Nevado-Filábride Complex, Betic Cordilleras, Spain), N Jb Geol Paläont Mh 7: 405–418

Gómez-Pugnaire MT, Franz G, López-Sánchez-Vizcaíno V (1994) Retrograde formation of NaCl-scapolite in high pressure metaevaporites from the Cordilleras Béticas (Spain), Contrib Mineral Petrol 116: 448–461

Gómez-Pugnaire MT, Braga JC, Martín JM, Sassi FP, Del Moro A (2000) The age of the Nevado-Filábride cover (Betic Cordilleras, S Spain) regional implications. Schweiz Mineral Petrogr Mitt 80: 45–52

Govindaraju K, Potts PJ, Webb PC, Watson JS (1994) Report on Whin Sill Dolerite WS-ER from England and Pitscurrie Microgabbro PM-S from Scotland: assessment by one hundred and four international laboratories. Geostand Newsl 18: 211–300

Gupta AK, Onuma K, Yagi K, Lidiak EG (1973) Effect of silica concentration on the diopsidic pyroxenes in the system diopside-$CaTiAl_2O_6SiO_2$. Contrib Mineral Petrol 41: 333–344

Hart SR, Davis KE (1978) Nickel partitioning between olivine and silicate melt. Earth Planet Sci Lett 40: 203–219

Hawkesworth CJ, Erlank AJ, Marsh JS, Menzies MA, Van Calsteren P (1983) Evolution of the continental lithosphere: evidence from volcanics and xenoliths in southern Africa. In: Hawkesworth CJ, Norry M (eds) Continental basalts and mantle xenoliths. Shiva Press, Nantwich Cheshire, pp 111–138

Hebeda EM, Boelrijk NAIM, Priem HNA, Vendurmen RH (1980) Excess radiogenic Ar and undisturbed Rb–Sr systems in basic intrusives subjected to Alpine metamorphism in SE Spain. Earth Planet Sci Lett 47: 81–90

Hergt JM, Peate DW, Hawkesworth CJ (1991) The petrogenesis of Gondwana low-Ti flood basalts. Earth Planet Sci Let 105: 134–148

Irvine TN, Baragar WRA (1971) A guide to chemical classification of common volcanic rocks. Can J Earth Sci 8: 523–548

Jabaloy A (1993) La estructura de la región occidental de la Sierra de los Filabres. PhD Thesis, University of Granada

Kawasaki T, Ito E (1994) An experimental determination of the exchange reaction of Fe^{2+} and Mg^{2+} between olivine and Ca-rich clinopyroxene. Am Mineral 79: 461–477

Lafuste MJ, Pavillon MJ (1976) Mise en évidence d'Eifélien daté au sein des terrains métamorphiques des zones internes des Cor. bétiques. CR Acad Sci Paris 283, série D: 1015–1018

Le Bas MJ, Le Maitre TW, Woolley AR (1992) The construction of the Total Alkali-Silica chemical classification of volcanic rocks. Mineral Petrol 48: 1–22

Leine L (1966) Rauwackes in the Betic Cordilleras, Spain. PhD Thesis, University of Amsterdam

Leterrier J, Maury RC, Thonon P, Girard D, Marchal M (1982) Clinopyroxene composition as a method of identification of the magmatic affinities of paleo-volcanic series. Earth Planet Sci Lett 59: 139–154

Li J, Kornprobst J, Vielzeuf D, Fabriès J (1995) An improved experimental calibration of the olivine-spinel geothermometer. Chinese J Geochemistry 14: 68–77

López-Sánchez-Vizcaíno V (1994) Evolución petrológica y geoquímica de las rocas carbonáticas en el área de Macaél-Cóbdar, Complejo Nevado-Filábride, SE España. PhD Thesis, University of Granada

López-Sánchez-Vizcaíno V, Franz G, Gómez-Pugnaire MT (1995) The behavior of Cr during metamorphism of carbonate rocks from the Nevado-Filábride Complex, Betic Cordilleras, Spain. Can Min 33: 85–104

Martínez-Martínez JM (1986) Evolución tectonometamórfica del complejo Nevado-Filábride en el sector de unión entre sierra Nevada y Sierra de los Filabres (Cordilleras Béticas), Cuad Geol 13: 1–19

Marzoli A, Renne PR, Piccirillo EM, Ernesto M, Bellieni G, De Min A (1999) Extensive 200-Million-year-old continental flood basalts of the Central Atlantic Magmatic Province. Science 284: 616–618.

McKenzie D, O'Nions RK (1995) The source region of the ocean island basalts. J Petrol 36: 133–159

Meschede M (1986) A method of discriminating between different types of mid-ocean ridges basalts and continental tholeiites with the Nb-Zr-Y diagram. Chem Geol 56: 207–218

Morata D, Puga E, Demant A, Aguirre L (1997) Geochemistry and tectonic setting of the "ophites" from the External Zones of the Betic Cordilleras (S Spain). Est Geol 53: 107–120

Morten L, Puga E (1984) Blades of olivine and orthopyroxene in ultramafic rocks from del Cerro del Almirez, Sierra Nevada Complex, Spain: relics of quench-textures harzburgites? N Jb Min Mh 5: 211–218

Morten L, Bargossi GM, Martínez-Martínez JM, Puga E, Díaz de Federico A (1987) Metagabbro and associated eclogites in the Lubrín area, Sierra Nevada complex, Spain. J Met Geol 5: 155–174

Muñoz M (1986) Estudio comparativo de los cuerpos intrusivos básicos asociados a los materiales de edad triásica de los dominios Subbético y Nevado-Filábride del sector centro-oriental de las Cordilleras Béticas. Geogaceta 1: 35–37

Muñoz M, Gómez-Pugnaire MT, Fernández-Soler JM (1988) Los clinopiroxenos de las metabasitas hipoabisales del Complejo Nevado-Filábride (Cordilleras Béticas), como indicadores de la afinidad magmática y del ambiente paleotectónico. II Congr Geol España 1: 425–433

Nijhuis HJ (1964) Plurifacial alpine metamorphism in the south-eastern Sierra de los Filabres, south of Lubrín, PhD Thesis, University of Amsterdam

Nisbet EG, Pearce JA (1977) Clinopyroxene composition in mafic lavas from different tectonic settings. Contrib Mineral Petrol 63: 149–160

Pearce JA (1982) Trace element characteristics of laves from destructive plate boundaries. In: Thorpe RS (ed.) Andesites. Wiley, New York, pp 525–528

Pearce JA, Cann JR (1973) Tectonic setting of basic volcanic rocks determined using trace elements analyses. Earth Planet Sci Lett 19: 290–300

Pearce JA, Parkinson IJ (1993) Trace elements model for mantle melting: application to volcanic arc petrogenesis. In: Princhard HM, Alabaster T, Harris N, Band Neary CR (eds) Magmatic processes and Plate Tectonics. Geol Soc Spec Publ 76: 373–404

Platt JP (1986) Dynamic of orogenic wedges and the uplift of high-pressure metamorphic rocks. Geol Soc Am Bull 9: 1037–1053

Platt JP, Behrmann JH (1986) Structures and fabrics in the crustal-scale shear zone, Betic Cordilleras, SE Spain. J Struct Geol 8: 15–34

Platt JP, Vissers RLM (1989) Extensional collapse of thickened continental lithosphere: A working hypothesis for the Alboran Sea and Gibraltar Arc. Geology 17: 540–543

Portugal Ferreira M, Ferreira JT, Puga E, Díaz de Federico A (1988) Geochronological contribution to the petrogenetic picture of the Betic Chain (SE Spain). II Congr Geol España 2: 55–58

Puga E, Díaz de Federico A, Fontboté JM (1974) Sobre la individualización y sistematización de las unidades profundas de la Zona Bética. Est Geol 30: 543–548

Puga E, Díaz de Federico A, Bargossi GM, Morten L (1989) The Nevado-Filábride metaophiolitic association in the Cóbdar region (Betic Cordillera, SE Spain) preservation of pillow structures and development of coronitic eclogites. Geod Acta 3: 17–36

Puga E, Díaz de Federico A, Demant A (1995) The eclogitized pillows of the Betic Ophiolitic Association: relics of the Tethys Ocean floor incorporated in the Alpine chain after subduction. Terra Nova 7: 31–43

Puga E, Nieto JM, Diaz de Federico A, Bodinier JL, Morten L (1999) Petrology and metamorphic evolution of ultramafic rocks and dolerite dykes of the Betic ophiolitic association (Mulhacén Complex, SE Spain); evidence of eo-Alpine subduction following an ocean-floor metasomatic process. Lithos 49: 23–56

Robinson JAC, Wood BJ, Blundy JD (1998) The beginning of melting of fertile and depleted peridotite at 1.5 GPa. Earth Planet Sci Lett 155: 97–111

Roeder PL, Emslie RF (1970) Olivine-liquid equilibrium. Contrib Mineral Petrol 29: 275–289

Schiffman P, Lofgren GE (1982) Dynamic crystallization studies on the Grande Ronde pillow basalts, central Washington. J Geol 90: 49–78

Shervais JW (1982) Ti-V plots and petrogenesis of modern and ophiolitic lavas. Earth Planet Sci Lett 59: 101–118

Simkin T, Smith JV (1970) Minor-element distribution in olivine. J Geol 78: 304–325

Sisson TW, Grove TL (1993) Experimental investigations of the role of H_2O in calc-alkaline differentiation and subduction zone magmatism. Contrib Mineral Petrol 113: 43–166

Soto JI (1993) Estructura y evolución metamórfica del Complejo Nevado-Filábride en la terminación oriental de la Sierra de los Filabres, Cordilleras Béticas. PhD Thesis, University of Granada

Spencer KJ, Lindsley DH (1981) A solution model for coexisting iron-titanium oxides. Am Mineral 66: 1189–1201

Sun SS, McDonough, WF (1989) Chemical and isotopic systematics of oceanic basalts: implications for mantle composition and processes In: Magmatism in the Ocean Basins. Saunders AD, Norry MJ (eds) Geol Soc Spec Publ 42: 313–345

Sweeney RJ, Duncan AR, Erlank AJ (1994) Geochemistry and petrogenesis of central Lebombo basalts of the Karoo igneous province. J Petrol 35: 95–125

Tendero JA, Martín-Algarra A, Puga E, Díaz de Federico A (1993) Lithostratigraphie des métasédiments de l'association ophiolitique Nevado-Filábride (SE Espagne) et mise en évidence d'objets ankéritiques évoquant des foraminifères du Crétacé: conséquences Palèogéographiques. CR Acad Sci Paris 316: 1115–1122

Thompson RN, Morrison MA (1988) Asthenospheric and lower-lithospheric mantle contributions to continental extensional magmatism; an example from the British Tertiary Province. Chem Geol 68: 1–15

Trommsdorff V, López-Sánchez-Vizcaíno V, Gómez-Pugnaire MT, Müntener O (1998) High-pressure breakdown of antigorite to spinifex-textured olivine and orthopyroxene, SE Spain. Contrib Mineral Petrol 132: 139–148

Ulmer P (1989) The dependence of the Fe^{2+} – Mg cation-partitioning between olivine and basaltic liquid on pressure, temperature and composition. An experimental study to 30 kbars. Contrib Mineral Petrol 101: 261–273

Vegas R, Muñoz M (1986) Sobre la evolución geodinámica del borde meridional de la Placa Ibérica. I Congr Español Geol: 105–118

Vissers RLM (1981) A structural study of the central Sierra de los Filabres (Betic Zone, SE Spain) with emphasis on deformational processes and their relation to the Alpine metamorphism. PhD Thesis, University of Amsterdam

Vissers RLM, Platt JP, van der Val D (1995) Late orogenic extension of the Betic Cordillera and the Alboran Domain: A lithospheric view. Tectonics 14: 786–803

Voet, HW (1967) Geological investigations in the northern Sierra de los Filabres around Macael and Cóbdar, south-eastern Spain, PhD Thesis, University of Amsterdam

Watts AB, Platt JP, Buhl P (1993) Tectonic evolution of the Alboran Sea basin. Basin Res 5: 153–177

Yoder HS, Tilley CE (1962) The origin of basalts magmas: an experimental study of natural and synthetic rocks system. J Petrol 3: 342–532

Zindler A, Hart S (1986) Chemical Geodynamics. Ann Rev Earth Planet Sci 14: 493–571